

Role of particle conservation in self-propelled particle systems

Christoph A. Weber, Florian Thüroff, Erwin Frey

Angaben zur Veröffentlichung / Publication details:

Weber, Christoph A., Florian Thüroff, and Erwin Frey. 2013. "Role of particle conservation in self-propelled particle systems." *New Journal of Physics* 15 (4): 045014.
<https://doi.org/10.1088/1367-2630/15/4/045014>.



PAPER • OPEN ACCESS

Role of particle conservation in self-propelled particle systems

To cite this article: Christoph A Weber *et al* 2013 *New J. Phys.* **15** 045014

View the [article online](#) for updates and enhancements.

You may also like

- [How to get the Nobel Prize in physics](#)
Carl Nordling
- [Si Dopant Behavior in InGaAs](#)
Kevin Scott Jones, Aaron Lind, Henry Aldridge et al.
- [Peer review declaration](#)

Role of particle conservation in self-propelled particle systems

Christoph A Weber¹, Florian Thüroff¹ and Erwin Frey²

Arnold Sommerfeld Center for Theoretical Physics and Center for NanoScience, Department of Physics, Ludwig-Maximilians-Universität München, Theresienstraße 37, D-80333 Munich, Germany
E-mail: frey@lmu.de

New Journal of Physics **15** (2013) 045014 (31pp)

Received 2 November 2012

Published 22 April 2013

Online at <http://www.njp.org/>

doi:10.1088/1367-2630/15/4/045014

Abstract. Actively propelled particles undergoing dissipative collisions are known to develop a state of spatially distributed coherently moving clusters. For densities larger than a characteristic value, clusters grow in time and form a stationary well-ordered state of coherent macroscopic motion. In this work we address two questions. (i) What is the role of the particles' aspect ratio in the context of cluster formation, and does the particle shape affect the system's behavior on hydrodynamic scales? (ii) To what extent does particle conservation influence pattern formation? To answer these questions we suggest a simple kinetic model permitting us to depict some of the interaction properties between freely moving particles and particles integrated in clusters. To this end, we introduce two particle species: single and cluster particles. Specifically, we account for coalescence of clusters from single particles, assembly of single particles on existing clusters, collisions between clusters and cluster disassembly. Coarse graining our kinetic model, (i) we demonstrate that particle shape (i.e. aspect ratio) shifts the scale of the transition density, but does not impact the instabilities at the ordering threshold and (ii) we show that the validity of particle conservation determines the existence of a longitudinal instability, which tends

¹ These authors contributed equally to this work.

² Author to whom any correspondence should be addressed.



Content from this work may be used under the terms of the [Creative Commons Attribution 3.0 licence](https://creativecommons.org/licenses/by/3.0/). Any further distribution of this work must maintain attribution to the author(s) and the title of the work, journal citation and DOI.

to amplify density heterogeneities locally, and in turn triggers a wave pattern with wave vectors parallel to the axis of macroscopic order. If the system is in contact with a particle reservoir, this instability vanishes due to a compensation of density heterogeneities.

Contents

1. Introduction	2
2. A coarse-grained kinetic model	4
2.1. Reaction equations	5
2.2. Constitutive equations	7
3. Derivation of hydrodynamic equations	8
3.1. Truncation scheme	9
3.2. Derivation of the hydrodynamic equations	10
4. Spatially homogeneous systems	14
4.1. Crossover to clustering	14
4.2. Homogeneous equations for momentum current density	16
5. Stability of inhomogeneous hydrodynamic equations	17
5.1. Linearization about stationary, spatially homogeneous base states	18
5.2. Stability of the disordered state $g_0 = 0$	19
5.3. Stability of the broken symmetry state $g_0 > 0$	21
6. Discussion and conclusion	24
Acknowledgments	27
Appendix A. Derivation of the Boltzmann collision cylinder for driven rods	27
Appendix B. Derivation of the gradient terms in the hydrodynamic equations	29
References	30

1. Introduction

The emergence of collective motion is a ubiquitous phenomenon in nature, encountered in a great variety of actively propelled systems [1–3]. Coherently moving groups have been observed over a broad range of length scales, spanning from micrometer-sized systems [4–10] over millimeter large granules [11–13] to large groups of animals [14]. The fact that the capability of synchronizing movements between agents is shared even among fundamentally different systems has called for abstract modeling approaches, aiming at identifying the essential properties of these systems both in terms of analytical descriptions [15–28] and by means of agent-based simulation techniques [29–39].

Theoretically, the emergence of collective motion has mostly been studied in the context of particle conserving systems. There are, however, a number of experimental systems in which the assumption of particle conservation is questionable. In typical gliding assays [4–6, 9, 10], for instance, collective motion of filaments is observed on a two-dimensional ‘motor carpet’ which itself is in contact with a three-dimensional bulk reservoir of filaments. However, the impact of particle conservation on the formation of patterns of collective motion remains largely elusive.

Here, we address the significance of constraints for particle number by highlighting the differences in the collective properties between particle conserving systems and those in contact

with a particle reservoir. Our focus will be on the comparison of two archetypical scenarios, which we will refer to as the *canonical* (particle conserving) and the *grand canonical* (violating particle conservation) scenarios, respectively.

To this end, we will resort to a kinetic approach, which has been set up previously by Aranson and Tsimring [16] to describe pattern formation in a system of interacting microtubules, and which has been extended to the case of self-propelled spheres by Bertin *et al* [17, 22]. In the following, we will extend this description in accordance with a physical picture of collective motion that has been developed over the last decade based on observations in agent-based simulations of locally interacting, particle conserving systems [31, 32, 37, 39]. Among the most pertinent phenomena that have been reported in the context of these studies is the formation of intricate local structures pervading these systems in the vicinity of the ordering transition. Densely packed cohorts of coherently moving particles—subsequently referred to as *clusters*—incessantly ‘nucleate’ and ‘evaporate’ on local scales, even below threshold, rendering the system isotropic and homogeneous only in the limit of macroscopic length scales. Individual particles exhibit superdiffusive behavior in this regime, performing quasi-ballistic ‘flights’ as long as they are part of a cluster, and conventional particle diffusion if they are not. Above threshold, collective motion manifests itself on macroscopic scales in the form of coherently moving and dense bands, which are submersed in an isotropic low-density ‘particle sea’. Spatially homogeneous flowing states, in contrast, are observed only well beyond the ordering threshold [31]. Moreover, particle geometry was demonstrated to play an essential role in the context of clustering dynamics, with higher aspect ratios facilitating the formation of clusters of coherently moving particles [37].

In the light of the above, we suggest a simplified modeling framework to incorporate the intricate role of clusters on the ordering behavior, which will be presented in greater technical detail in the following section. Particles interact via binary collisions with a scattering cross section that is explicitly derived as a function of particle shape. Depending on whether a given particle is part of a cluster or not, it will be associated with one of two distinct particle classes, which we will refer to as the class of *cluster particles* and the class of *single particles*, respectively. *Single particles* are ‘converted’ to *cluster particles* by ‘condensation’ every time a *single particle* collides with a cluster. Conversely, *cluster particles* are ‘converted’ back to *single particles* by an ‘evaporation’ process which we assume to occur at some constant (possibly particle shape dependent [37]) rate. Moreover, in the absence of interactions, *cluster particles* will be assumed to move ballistically, whereas *single particles* will be assumed to perform random walks. Taken together, the conversion dynamics and the class specificity of particle motion provide a simple way of implementing the typical superdiffusive behavior of individual particles, which was alluded to above. To assess the importance of particle conservation in the context of pattern formation, we will analyze two variants of this model. Firstly, we study closed systems in which the total number of particles is conserved (*canonical* scenario) and where, consequently, the denser cluster phase grows at the expense of the single phase. Secondly, we examine open systems in contact with a particle reservoir (*grand canonical* scenario), where the particle current out of the single phase is compensated so as to retain the density of the isotropic sea of *single particles* at a constant level; cf figure 1.

Our work is structured as follows. In section 2 the modeling framework for the *canonical* and *grand canonical* models is introduced and the model equations are discussed in detail. The corresponding hydrodynamic equations are derived in section 3 by means of an appropriate truncation scheme in Fourier space. Therein, we also give explicit expressions of

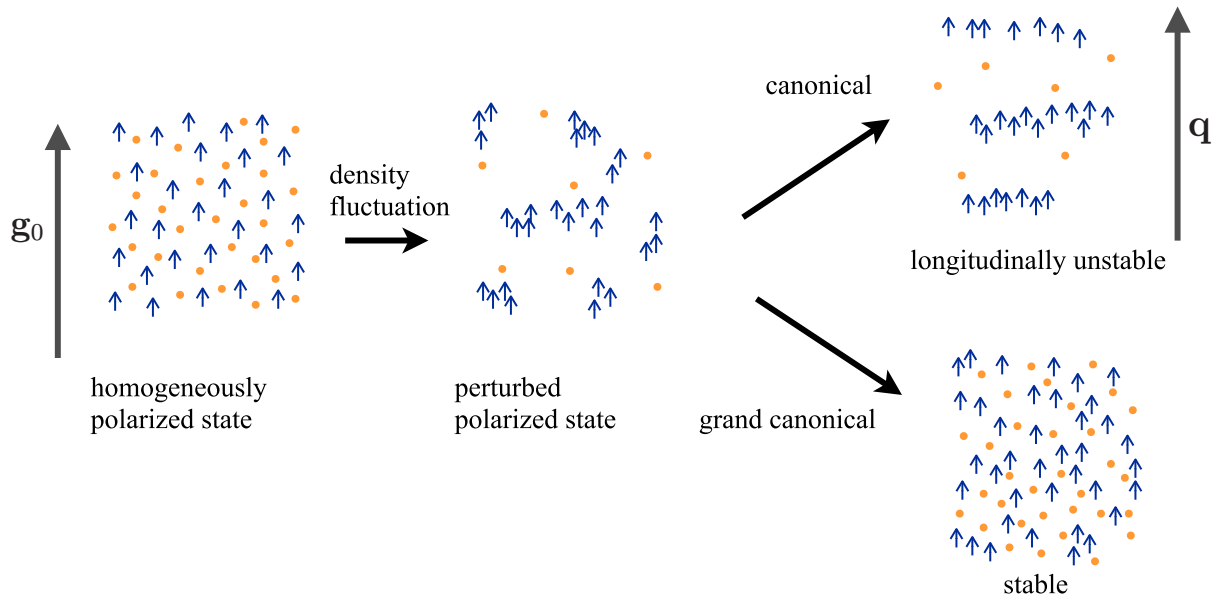


Figure 1. Illustration of the *canonical* and *grand canonical* modeling framework, highlighting the quintessential differences in the context of pattern formation. In the homogeneously polarized state (left), the *cluster particles* density (blue arrows) constitutes the system's macroscopic net momentum \mathbf{g}_0 , while some fraction of the system's particles, the *single particles* (orange dots), exhibit zero net momentum. Spatial perturbations of both density fields lead to two fundamentally different outcomes: (i) In the case of a closed system obeying total particle conservation (*single particles* + *cluster particles*), termed as the *canonical* model, the homogeneously polarized state is longitudinally unstable, with a wave vector \mathbf{q} parallel to the polarized state \mathbf{g}_0 , potentially enforcing a wave-like pattern. (ii) In contrast, open systems turn out to be stable against this kind of density fluctuation.

the kinetic coefficients as a function of the particles' aspect ratio and velocity, noise level and density for *single particles* and *cluster particles*. Section 4 is devoted to the analysis of the homogeneous equations. The dynamic's stationary fixed points are determined and the phase boundary between the isotropic and homogeneous states is calculated. Section 5 deals with the implications of the inhomogeneous equations in the framework of a linear stability analysis, which are concluded in section 6.

2. A coarse-grained kinetic model

We consider rod-like particles of length L and diameter d moving in two dimensions with a constant velocity v . A particle's state is determined by its position \mathbf{x} and the orientation θ of its velocity vector. To describe the time evolution of the system, we adopt a kinetic approach [16–18, 22].

On mesoscopic scales, the system's spatio-temporal evolution is then governed by Boltzmann-like equations for the one-particle distribution functions within the classes of *single*

particles and *cluster particles*, respectively. Interactions enter this description by means of collision integrals. The kernel of these integrals involves both a measure for the rate of collisions, as well as a ‘collision rule’ implementing a mapping between pre- and post-collisional directions θ and θ' of each of the two partaking particles. Here, we are led to consider a simplified model of binary particle interactions, which builds on the distinction between *single particles* and *cluster particles*. The details of this model will be described in the following section.

2.1. Reaction equations

Let $S(\theta)$ and $C(\theta)$ refer to a particle moving in the direction of θ and being associated with the class of *single particles* or *cluster particles*, respectively. In the absence of interactions, *single particles* are assumed to perform a persistent random walk, which we model as a succession of ballistic straight flights, interspersed by self-diffusion (‘tumble’) events. These tumble events are assumed to occur at a constant rate λ and reorient the particle’s orientation θ by a random amount ϑ_0 :

$$S(\theta) \xrightarrow{\lambda} S(\theta' = \theta + \vartheta_0). \quad (1)$$

For simplicity we assume ϑ_0 to be Gaussian distributed,

$$p_0(\vartheta_0) = \frac{1}{\sqrt{2\pi\sigma_0^2}} \exp(-\vartheta_0^2/2\sigma_0^2), \quad (2)$$

with σ_0 denoting the standard deviation. On time scales much larger than λ^{-1} , this tumbling behavior can be described as conventional particle diffusion, with the particles’ diffusion constant being a function of λ and σ_0 [40].

When two *single particles* $S(\theta_1)$ and $S(\theta_2)$ collide, they are assumed to assemble a cluster, i.e. each of the two particles becomes a *cluster particle* (see figure 2(a)):

$$S(\theta_1) + S(\theta_2) \rightarrow C(\bar{\theta} + \vartheta) + C(\bar{\theta} + \vartheta), \quad (3)$$

where³

$$\bar{\theta}(\theta_1, \theta_2) = \frac{1}{2}(\theta_1 + \theta_2) \quad (4)$$

denotes the average of both pre-collisional angles θ_1 and θ_2 , and where ϑ is a random variable which we, again, assume to be Gaussian distributed:

$$p(\vartheta) = \frac{1}{\sqrt{2\pi\sigma^2}} \exp(-\vartheta^2/2\sigma^2). \quad (5)$$

The rate of binary collisions, such as equation (3), is determined by a particle-shape-dependent *differential scattering cross section*, which will be discussed below; see section 2.2 and appendix A.

Collisions involving *cluster particles* are distinct from *single particle* events. Due to the close spatial proximity of particles within each cluster, these collisions correspond to many-particle interactions. Needless to say, a detailed description of cluster formation and the ensuing particle dynamics represents a highly complex matter, requiring explicit consideration of such

³ To make sure that $\bar{\theta}$ points into the ‘right’ direction (i.e. $|\bar{\theta} - \theta_{1/2}| \leq \pi/2$), we choose $\theta_1 \in (-\pi, \pi]$ and $\theta_2 \in (\theta_1 - \pi, \theta_1 + \pi]$.

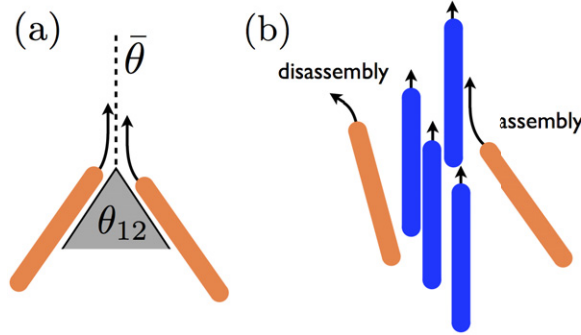


Figure 2. (a) Illustration of two *single particle* species (light orange) with a pre-collisional relative angle of θ_{12} , colliding such that they align collinear to the average angle $\bar{\theta}$. Both particles become a cluster species after the collision. (b) Right: illustration of a possible scenario where a single particle joins a cluster by perfectly aligning to the cluster particles (blue). Left: a particle leaves the cluster by a random change of its direction at a characteristic rate ϵ .

many-particle interactions. For simplicity, we will resort to the following simplified interaction picture. We assume that (binary) collisions between *single particles* and *cluster particles* lead to a condensation process during which the *single particle* aligns to the *cluster particle* without changing the direction of the cluster as a whole:

$$S(\theta_1) + C(\theta_2) \rightarrow C(\theta_2) + C(\theta_2). \quad (6)$$

Equation (6) thus captures the net effect of collisions between *single particles* and *cluster particles*, during which multiple collisions, involving neighboring particles belonging to the same cluster, stabilize the cluster's direction; cf figure 2(b) for an illustration.

Collisions among *cluster particles* is an even more intricate process, since they actually depend on the size and shape of both colliding clusters, and in general involve multi-particle interactions. In the framework of a Boltzmann-like description, correlations in the particle distribution are neglected and only binary interactions are considered. The frequency of interactions is determined by a geometrical construction called the 'Boltzmann cylinder', assuming that particle positions are homogeneously distributed on local scales. With regard to many-particle interactions during collisions among *cluster particles*, we thus have to resort to some kind of simplified, binary collision picture. Since our kinetic model lacks any direct notion of cluster size or shape, we will stick to the assumption that, on average, collisions between *cluster particles* are devoid of any directional bias, leading to the same type of collision rule as for *single particles*:

$$C(\theta_1) + C(\theta_2) \rightarrow C(\bar{\theta} + \vartheta) + C(\bar{\theta} + \vartheta). \quad (7)$$

Again, ϑ constitutes a Gaussian-distributed random variable given in (5). Moreover, due to external (e.g. thermal background) and internal (e.g. noisy propelling mechanism) noise, *cluster particles* evaporate to become *single particles*. In analogy to the self-diffusion of *single particles*, we thus introduce a rate⁴ ϵ characterizing the following evaporation process:

$$C(\theta) \xrightarrow{\epsilon} S(\theta' = \theta + \vartheta_0). \quad (8)$$

⁴ As has been pointed out in [37], this rate may depend on particle shape.

Also in this case, the strength of the angular changes is Gaussian distributed according to (2), and for simplicity we use the same standard deviation σ_0 as for the *single particles'* persistent random walk. As discussed above, *cluster particles* are strongly caged due to their close proximity to neighboring, collinearly moving particles. Reorientations of *cluster particles* due to noise are therefore strongly counteracted by realigning particle collisions, rendering *cluster particles* considerably less susceptible to random fluctuations than *single particles*. Hence, we assume

$$\epsilon \ll \lambda, \quad (9)$$

which is consistent with the observations in agent-based simulations slightly below the ordering transition [31], finding coherently moving clusters in an unpolarized background of randomly moving particles. In this regime individual particles exhibit superdiffusive behavior, performing quasi-ballistic ‘flights’ as long as they are part of a cluster, and conventional particle diffusion if they are not.

2.2. Constitutive equations

Building on the modeling framework defined above, we now set up a kinetic description for the *canonical* model. We denote by $s(\theta, \mathbf{x}, t)$ and $c(\theta, \mathbf{x}, t)$ the one-particle distribution functions within the class of *single particles* and *cluster particles*, respectively, i.e. $s(\theta, \mathbf{x}, t) d\theta d^2x$ gives the number of *single particles* located in an infinitesimal region $[\mathbf{x}, \mathbf{x} + d\mathbf{x}]$ with orientations in the interval $[\theta, \theta + d\theta]$ (and likewise for $c(\theta, \mathbf{x}, t) d\theta d^2x$). Both one-particle distribution functions are subject to convection due to the propelling velocity \mathbf{v} of each particle. Moreover, local fluctuations in the one-particle distribution functions due to self-diffusion and collision events are to be accounted for. We thus arrive at the following set of Boltzmann-like equations for the *canonical* model:

$$\partial_t s(\theta, \mathbf{x}, t) + \mathbf{v} \cdot \nabla s(\theta, \mathbf{x}, t) = \dot{s}(\theta, \mathbf{x}, t), \quad (10a)$$

$$\partial_t c(\theta, \mathbf{x}, t) + \mathbf{v} \cdot \nabla c(\theta, \mathbf{x}, t) = \dot{c}(\theta, \mathbf{x}, t), \quad (10b)$$

where the source terms $\dot{s}(\theta, \mathbf{x}, t)$ and $\dot{c}(\theta, \mathbf{x}, t)$ read

$$\dot{s} = \lambda [\mathcal{D}_s^{(+)}(\theta) - \mathcal{D}_s^{(-)}(\theta)] + \epsilon \mathcal{D}_c^{(+)}(\theta) - \mathcal{C}_s^{(-)}(\theta) - \mathcal{A}[s, c; \theta], \quad (11a)$$

$$\dot{c} = -\epsilon \mathcal{D}_c^{(-)}(\theta) + \mathcal{C}_s^{(+)}(\theta) + \mathcal{C}_c^{(+)}(\theta) + \mathcal{A}[c, s; \theta] - \mathcal{C}_c^{(-)}(\theta). \quad (11b)$$

They give the net number of *single particles* and *cluster particles* entering the phase space region $d\omega = [\mathbf{x}, \mathbf{x} + d\mathbf{x}] \times [\theta, \theta + d\theta]$ per unit time and unit area, respectively. The various terms correspond to gain (superscript $^{(+)}$) and loss (superscript $^{(-)}$) of particles by the following processes.

1. *Self-diffusion and evaporation.* In these cases the source terms are products of the corresponding rates and probability densities, with

$$\mathcal{D}_f^{(-)}(\theta) = f(\theta) \quad (12)$$

denoting the probability density for a particular species f to have a certain angle θ , and

$$\mathcal{D}_f^{(+)}(\theta) = \langle f(\theta - \vartheta_0) \rangle_0 \quad (13)$$

denoting the transition probability from $\theta' = \theta - \vartheta_0$ to θ averaged over all ϑ_0 with respect to the Gaussian weight (2). Note that, here and in the following, the argument of f is understood modulo 2π .

2. *Collisions within the same class of particles.* The collision integrals, representing the processes defined in equations (3) and (7), are given by standard expressions [16–18, 22]

$$\mathcal{C}_f^{(+)}(\theta) = \left\langle \int d\mathcal{I} f(\theta') f(\theta'') \delta(\bar{\theta}(\theta', \theta'') + \vartheta - \theta) \right\rangle, \quad (14a)$$

$$\mathcal{C}_f^{(-)}(\theta) = \int d\mathcal{I} f(\theta') f(\theta'') \delta(\theta' - \theta). \quad (14b)$$

Here $\langle \dots \rangle$ denotes an average over $\vartheta \in (-\infty, \infty)$ with respect to the Gaussian weight (5) and the average angle $\bar{\theta}$ is given in equation (4). The integral measure

$$\int d\mathcal{I} (\dots) \equiv \int_{-\pi}^{\pi} d\theta' \int_{\theta'-\pi}^{\theta'+\pi} d\theta'' \Gamma(L, d, |\theta' - \theta''|) (\dots) \quad (15)$$

contains the *differential scattering cross section*

$$\Gamma(L, d, |\theta' - \theta''|) = 4 dv \left| \sin \left(\frac{\theta' - \theta''}{2} \right) \right| \left[1 + \frac{(L/d) - 1}{2} |\sin(\theta' - \theta'')| \right] \quad (16)$$

characterizing the frequency of collisions (i.e. hard-core interactions) between rod-like particles. The scattering function Γ itself carries all information concerning the shape of the particles and is a function of the relative orientation of the colliding particles. Reminiscent of the Boltzmann scattering cylinder, Γ can be derived on the basis of purely geometric considerations assuming that all spatial coordinates within the cylinder are equally probable; for details see appendix A.

3. *Assembly events of a single particle joining a cluster.* These events, represented by (6), occur through binary collisions between *single particles* and *cluster particles* and are thus represented by an analogous integral expression:

$$\mathcal{A}[f, g; \theta] = \int d\mathcal{I} f(\theta') g(\theta'') \delta(\theta' - \theta). \quad (17)$$

3. Derivation of hydrodynamic equations

In order to reduce our kinetic description to a set of hydrodynamic equations valid on large length and time scales, we follow the well-established procedure of Aranson and Tsimring [16] and Bertin *et al* [17, 22], and analyze the angular dependence of equations (10a) and (10b) in Fourier space. Due to the 2π -periodicity in θ , the one-particle distribution functions can be expanded in Fourier series

$$s(\theta, \mathbf{x}, t) = \frac{1}{2\pi} \sum_{n=-\infty}^{\infty} s_n(\mathbf{x}, t) e^{-in\theta}, \quad (18a)$$

$$c(\theta, \mathbf{x}, t) = \frac{1}{2\pi} \sum_{n=-\infty}^{\infty} c_n(\mathbf{x}, t) e^{-in\theta}, \quad (18b)$$

where

$$s_n(\mathbf{x}, t) = \int_{-\pi}^{\pi} d\theta e^{in\theta} s(\theta, \mathbf{x}, t), \quad (19a)$$

$$c_n(\mathbf{x}, t) = \int_{-\pi}^{\pi} d\theta e^{in\theta} c(\theta, \mathbf{x}, t). \quad (19b)$$

Upon identifying $\mathbb{R}^2 \leftrightarrow \mathbb{C}$, e.g. $\mathbf{v} \leftrightarrow v e^{i\theta}$ ($v = |\mathbf{v}|$), the zeroth and first Fourier modes are directly connected to the hydrodynamic densities ρ_s (*single particle density*) and ρ_c (*cluster particle density*), and the corresponding current densities \mathbf{g}_s and \mathbf{g}_c , i.e.

$$\rho_s(\mathbf{x}, t) = s_0(\mathbf{x}, t), \quad (20a)$$

$$\rho_c(\mathbf{x}, t) = c_0(\mathbf{x}, t), \quad (20b)$$

$$\mathbf{g}_s(\mathbf{x}, t) \equiv \rho_s(\mathbf{x}, t) \mathbf{u}_s(\mathbf{x}, t) = v s_1(\mathbf{x}, t), \quad (20c)$$

$$\mathbf{g}_c(\mathbf{x}, t) \equiv \rho_c(\mathbf{x}, t) \mathbf{u}_c(\mathbf{x}, t) = v c_1(\mathbf{x}, t). \quad (20d)$$

In equations (20c) and (20d), the ‘=’ signs indicate identification of vectors and complex numbers. The quantities $\mathbf{u}_{s/c}$ denote the velocities of the macroscopic flow fields established by *single particles* and *cluster particles*, respectively. Also note that the second Fourier components are proportional to the nematic order parameter within the respective class of particles (as reflected by the symmetry of $e^{i2\theta}$ under $\theta \rightarrow \theta + \pi$). Using equations (18a) and (18b), the Boltzmann-like equations (10a) and (10b) transform to

$$\begin{aligned} \partial_t s_k + \frac{v}{2} [\partial_x (s_{k+1} + s_{k-1}) - i \partial_y (s_{k+1} - s_{k-1})] \\ = -\lambda s_k + e^{-(k\sigma_0)^2/2} (\lambda s_k + \epsilon c_k) - \sum_{n=-\infty}^{\infty} I_{n,0} (s_n + c_n) s_{k-n}, \end{aligned} \quad (21a)$$

$$\begin{aligned} \partial_t c_k + \frac{v}{2} [\partial_x (c_{k+1} + c_{k-1}) - i \partial_y (c_{k+1} - c_{k-1})] \\ = -\epsilon c_k + \sum_{n=-\infty}^{\infty} [I_{n,0} (s_n c_{k-n} - c_n c_{k-n}) + e^{-(k\sigma)^2/2} I_{n,k} (s_n s_{k-n} + c_n c_{k-n})], \end{aligned} \quad (21b)$$

where the collision integrals $I_{n,k}$ are defined as follows:

$$I_{n,k} = \frac{1}{2\pi} \int_{-\pi}^{\pi} d\phi \Gamma(L, d, |\phi|) \cos \left[\left(n - \frac{k}{2} \right) \phi \right]. \quad (22)$$

Note, in particular, that $I_{0,0}$ gives the *total scattering cross section*.

3.1. Truncation scheme

Equations (21a) and (21a) constitute an infinite set of coupled equations in Fourier space, which are fully equivalent to the Boltzmann-like equations (10a) and (10b). To derive a closed set of hydrodynamic equations, we need to consider some additional assumptions, allowing us to truncate this infinite Fourier space representation.

Here, our focus will be on virtually isotropic systems in the vicinity of an ordering transition breaking rotational symmetry. In this case, deviations of the one-particle distribution functions from the constant distribution $\sim 1/2\pi$ are small and contributions from large wavenumbers in the Fourier series (21a) and (21a) are negligible. We further consider sufficiently dilute systems, in which the number of (binary) particle collisions per unit time and area $[\sim (\rho_c + \rho_s)^2 I_{0,0}]$ is much smaller than the corresponding number of *single particle*

Table 1. Summary of relevant collision integrals $I_{n,k}$ as a function of the aspect ratio $\xi = L/d$, where L and d denote particle length and diameter, and where v is the particle velocity. The quantities $I_{n,k}/I_{0,0}$ depend only weakly on the aspect ratio ξ . In particular, the signs of $I_{n,k}/I_{0,0}$ do not change with ξ , leaving all our present conclusions made on the basis of the kinetic coefficients qualitatively unchanged.

Integral	$I_{0,0}$	$I_{1,0}/I_{0,0}$	$I_{1,1}/I_{0,0}$	$I_{2,0}/I_{0,0}$	$I_{2,1}/I_{0,0}$
Value	$\frac{8dv(2+\xi)}{3\pi}$	$-\frac{4+\xi}{5(2+\xi)}$	$\frac{3}{16} \frac{8+\pi(\xi-1)}{2+\xi}$	$\frac{6-13\xi}{35(2+\xi)}$	$\frac{3}{16} \frac{\pi(1-\xi)-8}{2+\xi}$

diffusion events [$\sim \lambda \rho_s$]. Together with $\epsilon \ll \lambda$ (equation (9)), stating that disassembly from a cluster is strongly hindered by particle caging, allows us to treat *single particle* diffusion as a fast process. The *single particle* phase thus acts as an isotropic sea of particles where particle orientations (but not necessarily particle densities) are equilibrated, and hence the net hydrodynamic flow vanishes ($\mathbf{u}_s = 0$). Finally, from a dimensional analysis of equations (19a) and (19b), together with (20c) and (20d), one finds $c_k/\rho_c \sim \mathcal{O}(|\mathbf{u}_c|^k/v^k)$. Near the onset of order, where $|\mathbf{u}_c|/v \ll 1$, we only consider the density (c_0) and polarity (c_1) of *cluster particles*, and use the stationary equation for c_2 as a closure relation, neglecting all contributions from higher order coefficients.

In summary, we resort to the following truncation scheme, leading to a set of hydrodynamic equations, valid near the onset of the ordering transition:

$$s_k = 0, \quad \forall |k| > 0, \quad (23a)$$

$$c_k = 0, \quad \forall |k| > 2. \quad (23b)$$

3.2. Derivation of the hydrodynamic equations

With the above truncation scheme, (21a) and (21b) reduce to

$$\partial_t s_0 = \epsilon c_0 - I_{0,0} (s_0^2 + s_0 c_0), \quad (24a)$$

$$\partial_t c_0 = -v [\partial_x \Re(c_1) + \partial_y \Im(c_1)] - \partial_t s_0, \quad (24b)$$

$$\begin{aligned} \partial_t c_1 = & -\frac{v}{2} [\partial_x (c_2 + c_0) - i \partial_y (c_2 - c_0)] + [(2e^{-\sigma^2/2} I_{1,1} - I_{1,0} - I_{0,0}) c_0 - \epsilon + I_{0,0} s_0] c_1 \\ & + [2e^{-\sigma^2/2} I_{2,1} - I_{1,0} - I_{2,0}] c_1^* c_2, \end{aligned} \quad (24c)$$

$$\begin{aligned} \partial_t c_2 = & -\frac{v}{2} [\partial_x + i \partial_y] c_1 + [(2e^{-2\sigma^2} I_{1,0} - I_{2,0} - I_{0,0}) c_0 - \epsilon + I_{0,0} s_0] c_2 \\ & + [e^{-2\sigma^2} I_{0,0} - I_{1,0}] c_1 c_1, \end{aligned} \quad (24d)$$

where we used $f_{-k} = f_k^*$, since $f(\theta) \in \mathbb{R}$ ($f \in \{s, c\}$), and where $\Re(a)$ ($\Im(a)$) denotes the real (imaginary) part of a . Moreover, as can be seen from the definition in (22), the collision integrals $I_{n,k}$ only depend on the value $|n - k/2|$, whence only five of the collision integrals appearing in the above equations are independent. These integrals as a function of the particle's aspect ratio are evaluated and summarized in table 1. Also note that the entire set of equations (24a)–(24d) is

independent of the fast *single particle* diffusion time scale λ^{-1} (and, hence, also of the diffusion noise parameter σ_0). In our present approach, λ has only a conceptual meaning in maintaining a well-mixed particle bath within the class of *single particles*.

For given particle densities, the time scales governing the dynamics of the polar and nematic order parameter fields, represented by c_1 and c_2 , are given by the linear coefficients in the second line of (24c) and (24d), respectively. As will be detailed in section 4.2, the onset of collective motion is hallmarked by a change in sign of the linear coefficient in (24c), implying a diverging time scale for the dynamics of the polarity field. On the other hand, the time scale for c_2 is finite for all densities, which implies that the relaxation of the nematic order parameter field is fast compared to the polarity field. This allows us to set $\partial_t c_2 \approx 0$ in (24d).

In the following, it will be convenient to write down equations in dimensionless form. To this end, we construct the following characteristic scales: time and space will be measured in units of the cluster evaporation time and length scale

$$\hat{\tau}_e = \epsilon^{-1} \quad \text{and} \quad \hat{\ell}_e = v/\epsilon. \quad (25)$$

From the cluster evaporation time scale $\hat{\tau}_e$ and the *total scattering cross section* $I_{0,0}$, we can construct the characteristic density scale

$$\hat{\rho}_b = \frac{1}{I_{0,0} \hat{\tau}_e}. \quad (26)$$

The *single particle* and *cluster particle* phases constantly exchange particles at rates that are determined by cluster evaporation (ϵ) on the one hand (*cluster particles* \rightarrow *single particles*) and cluster nucleation due to particle collisions on the other hand (*single particles* \rightarrow *cluster particles*) which occur with a rate $\sim \rho I_{0,0}$. Therefore the characteristic density scale $\hat{\rho}_b$ marks the particle density, where both rates balance. In particular, $\rho/\hat{\rho}_b = (\rho_s + \rho_c)/\hat{\rho}_b$ gives the rate of inter-particle collisions relative to cluster evaporation events. Thus, the numerical quantity $\rho/\hat{\rho}_b$ provides a direct measure expressing the competition between the randomizing effects of noise and the order creating effects of particle collisions, hallmarking the onset (and maintenance) of collective motion [29].

We thus arrive at the following rescaling scheme:

$$t \rightarrow t \cdot \hat{\tau}_e, \quad (27a)$$

$$\mathbf{x} \rightarrow \mathbf{x} \cdot \hat{\ell}_e, \quad (27b)$$

$$\rho_{s/c} \rightarrow \rho_{s/c} \cdot \hat{\rho}_b, \quad (27c)$$

$$\mathbf{g} \rightarrow \mathbf{g} \cdot \hat{\rho}_b \frac{\hat{\ell}_e}{\hat{\tau}_e}, \quad (27d)$$

$$I_{n,k} \rightarrow I_{n,k} \cdot \frac{1}{\hat{\rho}_b \hat{\tau}_e}, \quad (27e)$$

where the characteristic scales for momentum (\mathbf{g}) and scattering cross section ($I_{n,k}$) have been constructed from those of time, space and density. In this rescaling the momentum current density is equal to one if the corresponding fluid element with a characteristic density $\hat{\rho}_b$, for which cluster evaporation and nucleation balance, is convected with the particle velocity v .

Then, upon eliminating c_2 from (24c) as discussed above, and using the relations between Fourier modes and hydrodynamic fields (for details see appendix B), (20a)–(20d),

equations (24a)–(24d) give rise to the hydrodynamic equations corresponding to the *canonical model*. In rescaled variables they read

$$\partial_t \rho_s = \rho_c - (\rho_s + \rho_c) \rho_s, \quad (28a)$$

$$\partial_t \rho_c = -\nabla \cdot \mathbf{g} - \rho_c + (\rho_s + \rho_c) \rho_s, \quad (28b)$$

$$\begin{aligned} \partial_t \mathbf{g} = & -v_1 \mathbf{g} - \frac{\mu \kappa}{v_2} \mathbf{g}^2 \mathbf{g} - \frac{1}{2} \nabla \rho_c + \frac{1}{4v_2} \nabla^2 \mathbf{g} + \frac{\zeta_+}{v_2} (\mathbf{g} \cdot \nabla) \mathbf{g} + \frac{\zeta_-}{v_2} [(\nabla \cdot \mathbf{g}) \mathbf{g} - \frac{1}{2} \nabla(\mathbf{g}^2)] \\ & + \frac{\mu}{v_2^2} [\mathbf{g}(\mathbf{g} \cdot \partial[\rho_c, \rho_s]) - \frac{1}{2} \mathbf{g}^2 \partial[\rho_c, \rho_s]] + \frac{1}{4v_2^2} [(\nabla \cdot \mathbf{g}) \partial[\rho_c, \rho_s] \\ & - (\nabla \mathbf{g} + \nabla \mathbf{g}^t) \partial[\rho_c, \rho_s]], \end{aligned} \quad (28c)$$

where

$$\partial[f, g] = (\partial_f v_2) \nabla f + (\partial_g v_2) \nabla g, \quad (29)$$

and where we have introduced the following abbreviations:

$$v_1 = 1 - (\rho_s - \rho_c) + (I_{1,0} - 2e^{-\sigma^2/2} I_{1,1}) \rho_c, \quad (30a)$$

$$v_2 = 1 - (\rho_s - \rho_c) + (I_{2,0} - 2e^{-2\sigma^2} I_{1,0}) \rho_c, \quad (30b)$$

$$\mu = e^{-2\sigma^2} - I_{1,0}, \quad (30c)$$

$$\kappa = I_{1,0} + I_{2,0} - 2e^{-\sigma^2/2} I_{2,1}, \quad (30d)$$

$$\zeta_{\pm} = -\mu \pm \frac{\kappa}{2}. \quad (30e)$$

Equations (28a)–(28c) capture the evolution of our *canonical* model system on a hydrodynamic level. More specifically, (28a) and (28b) describe the spatio-temporal evolution of the particle densities ρ_s and ρ_c . Since, by the assumptions underlying our model, no macroscopic flow of *single particles* can build up, only the density of *cluster particles* (ρ_c) is subject to convection. This implies that the genuine hydrodynamic momentum field $\mathbf{g} = \mathbf{g}_c + \mathbf{g}_s \equiv \mathbf{g}_c$ is carried solely by the subset of cluster particles. Therefore we omit the subscript c in (28b) and (28c) and denote $\mathbf{g} \equiv \mathbf{g}_c$. The dynamics of both densities is, moreover, driven by source terms, as determined by the reactions discussed in section 2.1. The gain and loss parts in these source terms of ρ_c and ρ_s are exactly balanced, such that the total density $\rho = \rho_c + \rho_s$ is conserved. As an aside we note that any distinction between *single particles* and *cluster particles* is a purely conceptual matter. Experimentally, only the total density ρ and the momentum field \mathbf{g} are accessible.

Equation (28c), governing the evolution of the current density \mathbf{g} , can be interpreted as a generalization of the Navier–Stokes equation to active systems. The terms on the right-hand side of (28c) can be given by the following interpretation. In the first line, the first two terms account for the local dynamics of \mathbf{g} . They play a crucial role in establishing and maintaining a state of macroscopic flow, as will be detailed below. The Navier–Stokes equation itself, which conserves momentum, is devoid of these terms. In formal analogy to the Navier–Stokes equation, the density gradient in the first line together with the last term in the second line can be interpreted as a pressure gradient. This effective pressure is given by $\frac{1}{2}(\rho_c + \frac{\zeta_-}{v_2} \mathbf{g}^2)$, when neglecting the

density dependence of v_2 . The last term in the first line is analogous to the shear stress term in the Navier–Stokes equation, with a kinematic viscosity $\sim v_2^{-1}$. The second line in (28c) is a generalization of the convection term to systems not obeying Galilean invariance, where all combinations of ∇ and factors second order in \mathbf{g} transforming as vectors are allowed [41]. Finally, the last two lines describe couplings of the current density \mathbf{g} and gradients thereof to density gradients. Note that the density gradients in these coupling terms are all of the same generic structure (29).

As already noted, the *canonical* model equations (28a)–(28c) conserve the total number of particles. To make this explicit, we define

$$\rho \equiv \rho_c + \rho_s, \quad (31a)$$

$$\eta \equiv \rho_c - \rho_s, \quad (31b)$$

where ρ denotes the overall particle density and η measures the density difference between the two particle classes. The *canonical* model equations then attain the following form:

$$\partial_t \rho = -\nabla \cdot \mathbf{g}, \quad (32a)$$

$$\partial_t \eta = -\nabla \cdot \mathbf{g} + \rho^2 - (\rho + 1)\eta - \rho, \quad (32b)$$

$$\begin{aligned} \partial_t \mathbf{g} = & -v_1 \mathbf{g} - \frac{\mu\kappa}{v_2} \mathbf{g}^2 \mathbf{g} - \frac{1}{4} \nabla(\rho + \eta) + \frac{1}{4v_2} \nabla^2 \mathbf{g} + \frac{\zeta_+}{v_2} (\mathbf{g} \cdot \nabla) \mathbf{g} + \frac{\zeta_-}{v_2} \left[(\nabla \cdot \mathbf{g}) \mathbf{g} - \frac{1}{2} \nabla(\mathbf{g}^2) \right] \\ & + \frac{\mu}{v_2^2} \left[\mathbf{g}(\mathbf{g} \cdot \partial[\rho, \eta]) - \frac{1}{2} \mathbf{g}^2 \partial[\rho, \eta] \right] + \frac{1}{4v_2^2} [(\nabla \cdot \mathbf{g}) \partial[\rho, \eta] - (\nabla \mathbf{g} + \nabla \mathbf{g}^t) \partial[\rho, \eta]]. \end{aligned} \quad (32c)$$

The equation governing ρ expresses the overall conservation of particle number, whereas the source terms of equations (28a) and (28b) combine to determine the local dynamics of the relative density η in (32b).

Now we turn to the *grand canonical* model, where the *single particle* phase is coupled to a particle reservoir, resulting in a situation where *single particles* constitute an isotropic sea of particles that is maintained at a constant density ρ_s^0 . Particle number conservation is now violated, and the only non-trivial density dynamics takes place within the phase of *cluster particles*. The hydrodynamic equations corresponding to the *grand canonical* model can be obtained immediately by setting in (28a)–(28c) the density of *single particles* to a constant value, yielding

$$\rho_s = \rho_s^0 = \text{const.}, \quad (33a)$$

$$\partial_t \rho_c = -\nabla \cdot \mathbf{g} - \rho_c + (\rho_s^0 + \rho_c) \rho_s^0, \quad (33b)$$

$$\begin{aligned} \partial_t \mathbf{g} = & -v_1 \mathbf{g} - \frac{\mu\kappa}{v_2} \mathbf{g}^2 \mathbf{g} - \frac{1}{2} \nabla \rho_c + \frac{1}{4v_2} \nabla^2 \mathbf{g} + \frac{\zeta_+}{v_2} (\mathbf{g} \cdot \nabla) \mathbf{g} + \frac{\zeta_-}{v_2} \left[(\nabla \cdot \mathbf{g}) \mathbf{g} - \frac{1}{2} \nabla(\mathbf{g}^2) \right] \\ & + \frac{\mu \partial_{\rho_c} v_2}{v_2^2} \left[\mathbf{g}(\mathbf{g} \cdot \nabla \rho_c) - \frac{1}{2} \mathbf{g}^2 \nabla \rho_c \right] + \frac{\partial_{\rho_c} v_2}{4v_2^2} [(\nabla \cdot \mathbf{g}) \nabla \rho_c - (\nabla \mathbf{g} + \nabla \mathbf{g}^t) \nabla \rho_c]. \end{aligned} \quad (33c)$$

One final remark is in order. The rescaling scheme introduced in equations (27a)–(27e) renders both the *canonical* and *grand canonical* model equations virtually independent of particle shape.

While these equations exhibit a weak dependence on the particles' aspect ratio L/d (via the rescaled collision integrals $I_{n,k}$), this dependence introduces only minor quantitative effects, which are negligible for all present purposes. To a good approximation we can thus set $L/d = 1$ while working with dimensionless variables, and assess the effects entailed by particle shape by restoring original units. Within our present approach, the effects of particle shape are purely quantitative, causing a numerical shift in the characteristic scales, but leaving the qualitative features of the problem unaffected. Deep within the ordered phase, i.e. for large densities, we indeed find a qualitative change of the ensuing hydrodynamic instability, as detailed in section 5. Nevertheless, this statement has to be taken with a grain of salt because corresponding threshold densities are far beyond the validity of the hydrodynamic equations.

4. Spatially homogeneous systems

To investigate the implications of the hydrodynamic equations, we start with the simplest case by analyzing spatially homogeneous solutions. These considerations will provide the basis for the study of spatially inhomogeneous systems, which will be the subject of section 5. Dropping all gradients, the hydrodynamic equations for spatially homogeneous systems for the *canonical* model read

$$\partial_t \rho = 0, \quad (34a)$$

$$\partial_t \eta = \rho^2 - (\rho + 1)\eta - \rho, \quad (34b)$$

$$\partial_t \mathbf{g} = -v_1 \mathbf{g} - \frac{\mu\kappa}{v_2} \mathbf{g}^2 \mathbf{g}. \quad (34c)$$

For the *grand canonical* model we obtain

$$\partial_t \rho_c = -\rho_c + (\rho_s^0 + \rho_c) \rho_s^0, \quad (35a)$$

$$\partial_t \mathbf{g} = -v_1 \mathbf{g} - \frac{\mu\kappa}{v_2} \mathbf{g}^2 \mathbf{g}. \quad (35b)$$

In both cases, the density dynamics decouples from the momentum current dynamics and can be addressed separately.

In this section, our focus is on the stationary properties of the *canonical* and *grand canonical* models, respectively. While the dynamical approach to the stationary state is model dependent, the system's composition in terms of *single particles* and *cluster particles*, for given total density ρ , in the limit $t \rightarrow \infty$ is identical in both cases (refer to (28a)–(28b) and (33a)–(33b)). Since, moreover, the momentum current densities \mathbf{g} obey identical dynamical equations, the ensuing analysis of the stationary state is equal for both models.

4.1. Crossover to clustering

To assess the density difference between the *cluster particle* and the *single particle* phase η , we calculate the dynamical fixed point η^* of (34b), attracting the dynamics of $\eta(t)$ in the long time limit $t \rightarrow \infty$:

$$\eta^*(\rho) = \frac{\rho^2 - \rho}{\rho + 1}. \quad (36)$$

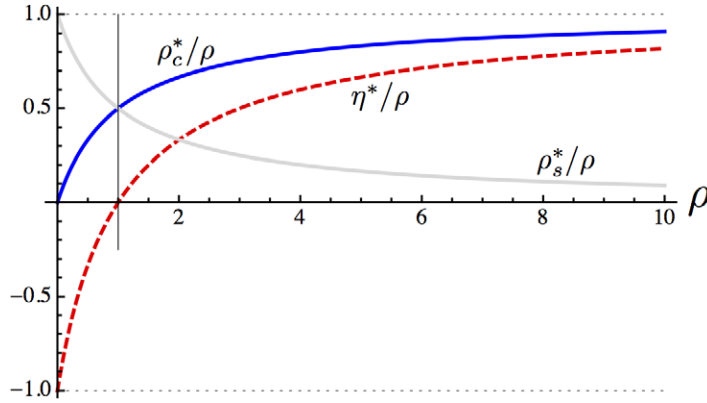


Figure 3. Fixed points of the homogeneous equations for the *grand canonical* and *canonical* models: the stationary relative density η^*/ρ , as well as the stationary cluster and single particle density, ρ_c^*/ρ and ρ_s^*/ρ , respectively. The larger the ρ , the more the cluster particles existing in the system. The vertical line corresponds to the density $\bar{\rho}$ above which the number of *cluster particles* exceeds the number of *single particles*. Note that $\rho_s < 1$ holds for all finite values of the total particle density ρ . (This is of particular relevance in the context of the *grand canonical* model, where ρ_s can be considered as a control parameter.)

The defining equations (31a)–(31b) can be used to determine the corresponding (stationary) fixed point densities of *single particles* (ρ_s^*) and *cluster particles* (ρ_c^*) as a function of the total density ρ . Figure 3 summarizes these findings. Upon increasing the total density ρ , the ratio η^*/ρ continuously grows from $\eta^*/\rho = -1$ at $\rho = 0$, asymptotically approaching $\eta^*/\rho = 1$ as $\rho \rightarrow \infty$. Based on the sign of η^* , two density regimes can be distinguished. In the low-density regime ($\rho \ll 1$, $\eta^* < 0$), particle collisions, underlying the formation of clusters, occur at much smaller rates than cluster evaporation events. Only a small fraction of all particles organize themselves in clusters, leading to a relatively dense population of *single particles* and a correspondingly small density of *cluster particles*. In the high-density regime ($\rho \gg 1$, $\eta^* > 0$), the situation is reversed: large overall densities imply frequent particle collisions and, consequently, cluster formation and cluster growth dominate over cluster evaporation. In this regime, the number of *cluster particles* exceeds the number of *single particles*.

The crossover between the *single particle* dominated low-density regime and the *cluster particle* dominated high-density regime occurs at the crossover density $\bar{\rho} = \hat{\rho}_b = 1$, where both the *single particle* and the *cluster particle* populations are of equal size (i.e. $\eta^*(\bar{\rho}) = 0$). The relation between the crossover density to clustering, and the geometrical shape of the constituent particles has been addressed previously in [37], based on agent-based simulations and a mean-field-type analytical analysis. Using our definition of the crossover density $\bar{\rho}$, we can establish the corresponding relation simply by restoring original units (equation (26)). Using packing fraction $\bar{p} \simeq \bar{\rho} Ld$ instead of particle density, and assuming for the sake of simplicity $L/d \gg 1$, which allows us to estimate the particle surface $A_0 \simeq Ld$, we find that

$$\bar{p} \simeq \frac{\epsilon Ld}{I_{0,0}} = \frac{3\pi}{8v} \frac{\epsilon L}{2 + L/d}, \quad (37)$$

which correctly reproduces the findings of [37] (taking into account that the cluster evaporation rate is assumed to be proportional to the inverse particle length, $\epsilon \propto L^{-1}$). For the sake of completeness, we note that the definition of the clustering crossover density in [37] is based on the cluster size distribution, and thus does not necessarily coincide with our definition. We stress, however, that in our description the scaling structure in equation (37) is completely generic. It is an immediate consequence of the characteristic scales of our model and of the fact that the rescaled hydrodynamic model equations are (virtually) independent of particle shape. The structure of equation (37) is thus robust under an arbitrary redefinition of the (rescaled) crossover density $\bar{\rho}$.

4.2. Homogeneous equations for momentum current density

Having examined the composition of the system in terms of *single particle* and *cluster particle* densities, we now turn to a discussion of the spatially homogeneous solutions for the momentum current density \mathbf{g} . Due to rotational invariance of (34c), only the magnitude $g = |\mathbf{g}|$ of the momentum current density, but not its direction, evolves in time. We can thus concentrate on the scalar equation

$$\partial_t g = -\nu_1 g - \frac{\mu\kappa}{\nu_2} g^3, \quad (38)$$

which leads to the following fixed points g^* as the attractor of the dynamics of g in the limit of long times:

$$g^* = \begin{cases} 0 & \text{for } \nu_1 > 0, \\ g_0 = \sqrt{-\frac{\nu_1 \nu_2}{\mu\kappa}} & \text{for } \nu_1 < 0. \end{cases} \quad (39)$$

It can be shown that the coefficient in front of the cubic term in (38) is indeed strictly positive for all control parameters of density ρ and noise σ consistent with $\nu_1 < 0$, ensuring the existence of the non-trivial fixed point in the second line of (39).

Depending on the sign of the linear coefficient ν_1 , two parameter regimes can thus be distinguished. Parameters leading to $\nu_1 > 0$ render stable an overall homogeneous and isotropic state with vanishing macroscopic flow $\mathbf{g} = 0$. Upon crossing the *phase boundary*

$$\nu_1(\rho, \sigma) = 0 \quad (40)$$

in parameter space, the isotropic solution gets unstable and a macroscopic current density of non-zero amplitude builds up. In equation (40) we used the fact that the density difference η , in the stationary limit, is a function of the total density ρ ; cf equation (36). Hence, in the limit of long times, ν_1 is a function of the total density ρ and the noise parameter σ , only.

Using the definition of the coefficient ν_1 , equation (30a), we can readily calculate the shape of the phase boundary in the $\sigma\rho$ -plane:

$$\sigma_c(\rho) = \sqrt{-2 \ln \left(\frac{2}{3} + \rho^{-2} \right)} \quad (\rho \geq \sqrt{3}), \quad (41)$$

where we used $I_{1,0} = -\frac{1}{3}$ and $I_{1,1} = \frac{1}{2}$. The corresponding phase diagram is shown in figure 4.

To conclude this section, we note that the analysis of spatially homogeneous systems corroborates the general physical picture of active systems, which was alluded to in the introduction (e.g. cf [31]). Even in the absence of noise, $\sigma = 0$, for which the threshold

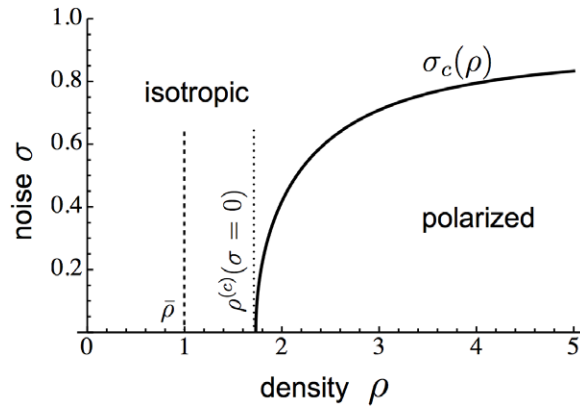


Figure 4. Phase diagram given by the homogeneous equations for the *canonical* and *grand canonical* models. For noise values smaller than the critical value, $\sigma < \sigma_c$, the isotropic state becomes unstable, giving rise to a state of collective motion of non-zero macroscopic momentum current. For $\sigma > \sigma_c$ the isotropic state ($g_0 = 0$) represents a stable solution. The vertical dotted line indicates the transition density $\rho^{(c)}$ at zero collision noise $\sigma = 0$, and the vertical dashed line corresponds to the crossover density $\bar{\rho}$, above which the number of *cluster particles* exceeds the number of *single particles*.

density $\rho^{(c)}$ is lowest, the fully isotropic state $\mathbf{g} = 0$ remains stable up to a critical density $\rho^{(c)}(\sigma = 0) = \sqrt{3} \bar{\rho}$, which lies well beyond the density $\bar{\rho}$ indicating the crossover to clustering. We thus extract the following physical picture; cf figure 4. For low densities, $\rho < \bar{\rho}$, cluster evaporation dominates over cluster assembly via particle collisions and clusters form only transiently. The system most closely resembles a structureless, isotropic ‘sea of particles’. At intermediate densities, $\bar{\rho} < \rho < \rho^{(c)}$, particle collisions are more frequent. The emergence of clusters is now a virtually persistent phenomenon, with cluster evaporation occurring at a lower rate than cluster formation and growth. Yet, the collision rates between clusters (i.e. collisions among *cluster particles*) are still too low to orchestrate macroscopic order, leading to an overall isotropic ‘sea of clusters’. Finally, for large densities, $\rho > \rho^{(c)}$, the frequency of collisions among clusters is high enough to establish collective motion even on macroscopic scales.

5. Stability of inhomogeneous hydrodynamic equations

From our discussions hitherto, we have ascertained that the isotropic, homogeneous state ($\rho = \text{const.}$ and $\mathbf{g} = 0$) becomes unstable for sufficiently large densities. Yet, from a purely homogeneous analysis we cannot say anything about the spatial structure of such a macroscopic broken-symmetry state. Nor can we be sure that the isotropic and homogeneous solution for $\rho < \rho^{(c)}(\sigma)$ is indeed stable with respect to spatially inhomogeneous perturbations. In this section, we therefore test the linear stability of the homogeneous isotropic and non-isotropic base states with respect to wave-like perturbations of arbitrary wavenumber. Unlike the homogeneous model equations, the full hydrodynamic model equations are different for both the *canonical* and *grand canonical* models, implying different dispersion relations describing the growth of such wave-like perturbations. We will thus analyze both models separately, and show that particle conservation does indeed influence pattern formation in essential respects.

5.1. Linearization about stationary, spatially homogeneous base states

We start by linearizing the hydrodynamic equations for the *canonical* model. In the *canonical* model, the total number of particles is conserved, and the appropriate base state reads (cf section 4)

$$\rho = \rho_h = \text{const.}, \quad (42a)$$

$$\eta = \eta^*(\rho_h) = \frac{\rho_h^2 - \rho_h}{\rho_h + 1}, \quad (42b)$$

$$\mathbf{g} = \mathbf{g}_h \in \left\{ 0, g_0 = \sqrt{-\frac{\nu_1 \nu_2}{\mu \kappa}} \right\} \hat{\mathbf{e}}_g, \quad (42c)$$

where $\hat{\mathbf{e}}_g$ denotes the unit vector in the direction of the homogeneous polarization, and where all fields of the base states are assumed to be constant in both space and time. We are going to investigate the linear stability of the solutions (42a)–(42c) against wave-like perturbations, employing the following ansatz:

$$\rho(\mathbf{x}, t) = \rho_h + \delta\rho(\mathbf{x}, t), \quad (43a)$$

$$\eta(\mathbf{x}, t) = \eta^* + \delta\eta(\mathbf{x}, t), \quad (43b)$$

$$\mathbf{g}(\mathbf{x}, t) = \mathbf{g}_h + \delta\mathbf{g}(\mathbf{x}, t), \quad (43c)$$

where the perturbations are plane waves

$$\delta\rho(\mathbf{x}, t) = \delta\rho_0 e^{st+i\mathbf{q}\cdot\mathbf{x}}, \quad (44a)$$

$$\delta\eta(\mathbf{x}, t) = \delta\eta_0 e^{st+i\mathbf{q}\cdot\mathbf{x}}, \quad (44b)$$

$$\delta\mathbf{g}(\mathbf{x}, t) = \delta\mathbf{g}_0 e^{st+i\mathbf{q}\cdot\mathbf{x}}. \quad (44c)$$

In the equations above, \mathbf{q} denotes the wave vector and s is the growth rate. Inserting this ansatz into the hydrodynamic equations (32a)–(32c), we obtain the following eigenvalue problem:

$$s \delta\rho_0 = -i\mathbf{q} \cdot \delta\mathbf{g}_0, \quad (45a)$$

$$s \delta\eta_0 = (2\rho_h - \eta^* - 1) \delta\rho_0 - (1 + \rho_h) \delta\eta_0 - i\mathbf{q} \cdot \delta\mathbf{g}_0, \quad (45b)$$

$$\begin{aligned} s \delta\mathbf{g}_0 = & \left[\frac{\partial_\rho \nu_2 \mu}{\nu_2^2} \left(\kappa \mathbf{g}_h^2 \mathbf{g}_h + (\mathbf{g}_h \cdot i\mathbf{q}) \mathbf{g}_h - \frac{i\mathbf{q}}{2} \mathbf{g}_h^2 \right) - \partial_\rho \nu_1 \mathbf{g}_h - \frac{i\mathbf{q}}{4} \right] \delta\rho \\ & + \left[\frac{\partial_\eta \nu_2 \mu}{\nu_2^2} \left(\kappa \mathbf{g}_h^2 \mathbf{g}_h + (\mathbf{g}_h \cdot i\mathbf{q}) \mathbf{g}_h - \frac{i\mathbf{q}}{2} \mathbf{g}_h^2 \right) - \partial_\eta \nu_1 \mathbf{g}_h - \frac{i\mathbf{q}}{4} \right] \delta\eta \\ & + \left[\frac{\zeta_+}{\nu_2} (i\mathbf{q} \cdot \mathbf{g}_h) - \frac{\mathbf{q}^2}{4\nu_2} - \nu_1 - \frac{\mu\kappa}{\nu_2} \mathbf{g}_h^2 \right] \delta\mathbf{g}_0 - \frac{2\mu\kappa}{\nu_2} \mathbf{g}_h (\mathbf{g}_h \cdot \delta\mathbf{g}_0) \\ & + \frac{\zeta_-}{\nu_2} [\mathbf{g}_h (i\mathbf{q} \cdot \delta\mathbf{g}_0) - i\mathbf{q} (\mathbf{g}_h \cdot \delta\mathbf{g}_0)]. \end{aligned} \quad (45c)$$

Unlike the *canonical* model, the *grand canonical* model conserves the number of *single particles*, but not the total number of particles. The appropriate base state in this case reads

$$\rho_s = \text{const.}, \quad (46a)$$

$$\rho_c = \rho_c^*(\rho_s) = \frac{\rho_s^2}{1 - \rho_s}, \quad (46b)$$

$$\mathbf{g} = \mathbf{g}_h \in \left\{ 0, g_0 = \sqrt{-\frac{\nu_1 \nu_2}{\mu \kappa}} \right\} \hat{\mathbf{e}}_g. \quad (46c)$$

We investigate the linear stability of these solutions, using a perturbation ansatz analogous to equations (43a)–(44c):

$$\rho_c(\mathbf{x}, t) = \rho_c^* + \delta\rho_c(\mathbf{x}, t), \quad (47a)$$

$$\mathbf{g}(\mathbf{x}, t) = \mathbf{g}_h + \delta\mathbf{g}(\mathbf{x}, t), \quad (47b)$$

with

$$\delta\rho_c(\mathbf{x}, t) = \delta\rho_c^0 e^{st+i\mathbf{q}\cdot\mathbf{x}}, \quad (48a)$$

$$\delta\mathbf{g}(\mathbf{x}, t) = \delta\mathbf{g}_0 e^{st+i\mathbf{q}\cdot\mathbf{x}}. \quad (48b)$$

Inserting this ansatz into equations (33a)–(33c), we obtain

$$s \delta\rho_c^0 = (\rho_s - 1) \delta\rho_c^0 - i\mathbf{q} \cdot \delta\mathbf{g}_0, \quad (49a)$$

$$\begin{aligned} s \delta\mathbf{g}_0 = & \left[\frac{\partial_{\rho_c} \nu_2 \mu}{\nu_2^2} \left(\kappa \mathbf{g}_h^2 \mathbf{g}_h + (\mathbf{g}_h \cdot i\mathbf{q}) \mathbf{g}_h - \frac{i\mathbf{q}}{2} \mathbf{g}_h^2 \right) - \partial_{\rho_c} \nu_1 \mathbf{g}_h - \frac{i\mathbf{q}}{2} \right] \delta\rho_c^0 \\ & + \left[\frac{\zeta_+}{\nu_2} (i\mathbf{q} \cdot \mathbf{g}_h) - \frac{\mathbf{q}^2}{4\nu_2} - \nu_1 - \frac{\mu\kappa}{\nu_2} \mathbf{g}_h^2 \right] \delta\mathbf{g}_0 - \frac{2\mu\kappa}{\nu_2} \mathbf{g}_h (\mathbf{g}_h \cdot \delta\mathbf{g}_0) \\ & + \frac{\zeta_-}{\nu_2} \left[\mathbf{g}_h (i\mathbf{q} \cdot \delta\mathbf{g}_0) - i\mathbf{q} (\mathbf{g}_h \cdot \delta\mathbf{g}_0) \right]. \end{aligned} \quad (49b)$$

5.2. Stability of the disordered state $g_0 = 0$

We start by considering the homogeneous and isotropic base states, which was shown to be stable against spatially homogeneous perturbations for $\rho < \rho^{(c)}(\sigma)$; cf section 4.2. To assess the stability of this state with respect to perturbations of arbitrary (non-zero) wave vectors in the *canonical* model, we use the linearized hydrodynamic equations (45a)–(45c) with $g_h = 0$. The resulting eigenvalue problem is most conveniently expressed in matrix form:

$$s \begin{pmatrix} \delta\rho_0 \\ \delta\eta_0 \\ \delta g_0 \end{pmatrix} = \begin{pmatrix} 0 & 0 & -iq \\ 2\rho_h - \eta^* - 1 & -(1 + \rho_h) & -iq \\ -iq/4 & -iq/4 & -\nu_1 - q^2/(4\nu_2) \end{pmatrix} \begin{pmatrix} \delta\rho_0 \\ \delta\eta_0 \\ \delta g_0 \end{pmatrix}. \quad (50)$$

The corresponding eigenvalue problem for the *grand canonical* model is found from equations (49a)–(49b), and attains the following form:

$$s \begin{pmatrix} \delta\rho_c^0 \\ \delta g_0 \end{pmatrix} = \begin{pmatrix} (\rho_s - 1) & -iq \\ -iq/2 & -\nu_1 - q^2/(4\nu_2) \end{pmatrix} \begin{pmatrix} \delta\rho_c^0 \\ \delta g_0 \end{pmatrix}. \quad (51)$$

For $\mathbf{g}_h = 0$, (45c) or (49b), respectively, implies $\mathbf{q} \parallel \delta\mathbf{g}_0$, allowing us to replace the vectors \mathbf{q} and $\delta\mathbf{g}_0$ by their respective magnitudes q and δg_0 . We solved both eigenvalue problems numerically for arbitrary wavenumbers $q > 0$ with the results shown in figure 5. Note that in

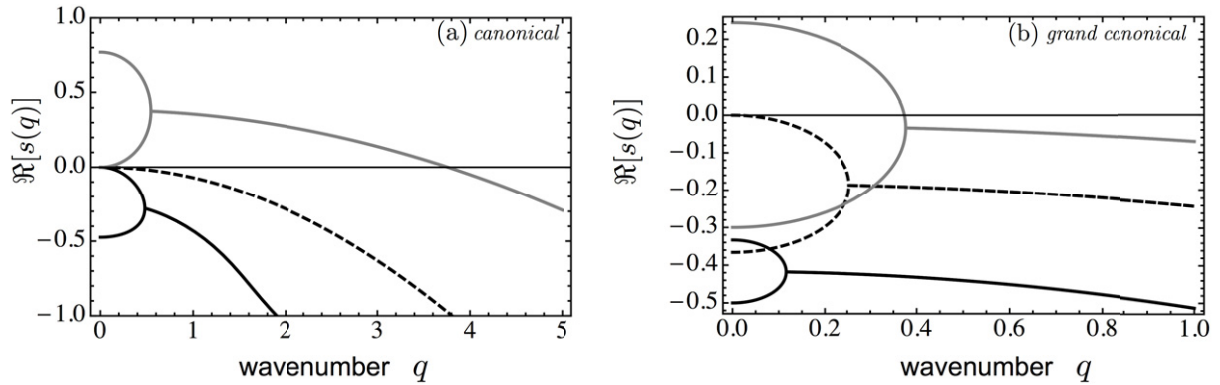


Figure 5. Fastest growth rate of $\Re[s(q)]$ as a function of the wavenumber $q = |\mathbf{q}|$ for the *canonical* (a) and *grand canonical* models (b), each for $\sigma = 0$. The disordered state is stable for all wavenumbers q if $\rho < \rho^{(c)}(\sigma)$. The marginal case, $\rho = \rho^{(c)}(\sigma)$, is dashed. An instability (gray) occurs for densities larger than the corresponding homogeneous critical density $\rho^{(c)}(\sigma)$. Similar behavior is found for $\sigma \neq 0$.

both models the real parts of all eigenvalues are negative for all wavenumbers $q > 0$, provided the particle density $\rho < \rho^{(c)}$. The spatially homogeneous, isotropic state is thus stable against small perturbations with *arbitrary* wave vectors.

For densities $\rho > \rho^{(c)}$, in contrast, a narrow band of positive eigenvalues emerges in both models, located at wavenumbers $q \ll 1$. Equations (50) and (51) evaluated at $q = 0$ return nothing but the linearized versions of the homogeneous hydrodynamic equations, (34a)–(34c) and (35a)–(35b). To gain new insights, we will therefore examine the limit $q \rightarrow 0$ and consider the eigenvalues of the above coefficient matrices to leading order in the wavenumber q .

In this limit of small wavenumbers, the *grand canonical* coefficient matrix, given in (51), approaches diagonal form and the dynamics of density fluctuations $\delta\rho_c^0$ and momentum current density fluctuations δg_0 practically decouple. Since $\rho_s < 1$ (cf figure 3), the first eigenvalue $s_1^{(\text{gc})} = \rho_s - 1 + \mathcal{O}(q^2)$ is strictly negative and density fluctuations decay exponentially. The second eigenvalue, $s_2^{(\text{gc})} = -\nu_1 + \mathcal{O}(q^2)$, is positive at small wavenumbers, leading to an instability in the momentum current density against long-wavelength fluctuations.

In the case of the *canonical* model (50), the coefficient matrix approaches block diagonal form in the limit of small wavenumbers. Again, the dynamics of momentum current density fluctuations δg_0 practically decouples from density fluctuations ($\delta\rho_0$ and $\delta\eta_0$), with momentum current density fluctuations being amplified by virtue of a positive eigenvalue $s_3^{(c)} = -\nu_1 + \mathcal{O}(q^2)$ at small wavenumbers. In contrast to the *grand canonical* model, however, particle conservation entails a marginally stable mode $s_1^{(c)}(q = 0) = 0$, which turns positive for $q \gtrsim 0$: $s_1^{(c)} \propto q^2$ (the remaining eigenvalue $s_2^{(c)} = -(1 + \rho_h) + \mathcal{O}(q^2)$ is strictly negative).

To sum up, the study of the linear stability of the homogeneous, isotropic state against spatially inhomogeneous perturbations of arbitrary wave vectors strongly suggests that particle conservation plays a vital role in the context of pattern formation. Both models exhibit spontaneous symmetry breaking by establishing a state of macroscopic collective motion. In the canonical model, in addition, conservation of total particle number entails a marginally stable density mode at $q = 0$ which is absent in the *grand canonical* model. This mode, in turn, gives

rise to a density instability at small, non-zero wavenumbers, accompanying the spontaneous symmetry breaking event for $\rho > \rho^{(c)}$. We note, however, that, at this point of the discussions, the existence of a narrow band of unstable modes at small wavenumbers does not allow for any conclusions concerning the structure of the macroscopic density and momentum current density for $\rho > \rho^{(c)}$. We will address this issue in greater detail in the following section.

5.3. Stability of the broken symmetry state $g_0 > 0$

Both the *canonical* and *grand canonical* models exhibit spontaneous symmetry breaking for overall densities $\rho > \rho^{(c)}(\sigma)$. To shed light on the spatial structure of this broken symmetry state, we start from the most simple case of a spatially homogeneous state of collective motion, and examine its stability with respect to wave-like perturbations in the hydrodynamic particle and momentum current densities. Without loss of generality, we assume that the direction of the macroscopic momentum current density coincides with the x -direction and choose $\mathbf{g}_h = g_0 \hat{\mathbf{e}}_x$. The wave vector \mathbf{q} of the perturbation fields is assumed to make an angle ψ with the macroscopic momentum current density \mathbf{g}_h , yielding $\psi = \angle(\mathbf{q}, \mathbf{e}_x)$ and $\mathbf{q} = q(\cos(\psi), \sin(\psi))$ with $q = |\mathbf{q}|$.

The linearized *canonical* model equations (45a)–(45c) then attain the following form:

$$s \delta \rho_0 = -iq \cos(\psi) \delta g_{x,0} - iq \sin(\psi) \delta g_{y,0}, \quad (52a)$$

$$s \delta \eta_0 = (2\rho_h - \eta^*(\rho_h) - 1) \delta \rho_0 - (1 + \rho_0) \delta \eta_0 - iq \cos(\psi) \delta g_{x,0} - iq \sin(\psi) \delta g_{y,0}, \quad (52b)$$

$$\begin{aligned} s \delta g_{x,0} = & \left[\frac{1}{2} iq \cos(\psi) \left(g_0^2 \frac{\mu}{v_2^2} \partial_\rho v_2 - \frac{1}{2} \right) - g_0 \left(\partial_\rho v_1 - \frac{\mu\kappa}{v_2^2} g_0^2 \partial_\rho v_2 \right) \right] \delta \rho_0 \\ & + \left[\frac{1}{2} iq \cos(\psi) \left(g_0^2 \frac{\mu}{v_2^2} \partial_\eta v_2 - \frac{1}{2} \right) - g_0 \left(\partial_\eta v_1 - \frac{\mu\kappa}{v_2^2} g_0^2 \partial_\eta v_2 \right) \right] \delta \eta_0 \\ & + \left(iq \cos(\psi) \frac{\zeta_+}{v_2} g_0 - \frac{q^2}{4v_2} - \frac{2\mu\kappa}{v_2} g_0^2 \right) \delta g_{x,0} + iq \frac{\zeta_-}{v_2} \sin(\psi) g_0 \delta g_{y,0}, \end{aligned} \quad (52c)$$

$$\begin{aligned} s \delta g_{y,0} = & -\frac{1}{2} iq \sin(\psi) \left(g_0^2 \frac{\mu}{v_2^2} \partial_\rho v_2 + \frac{1}{2} \right) \delta \rho_0 - \frac{1}{2} iq \sin(\psi) \left(g_0^2 \frac{\mu}{v_2^2} \partial_\eta v_2 + \frac{1}{2} \right) \delta \eta_0 \\ & - iq \sin(\psi) \frac{\zeta_-}{v_2} g_0 \delta g_{x,0} + \left(iq \cos(\psi) \frac{\zeta_+}{v_2} g_0 - \frac{q^2}{4v_2} \right) \delta g_{y,0}. \end{aligned} \quad (52d)$$

The corresponding equations for the *grand canonical* model read

$$s \delta \rho_c^0 = (\rho_s - 1) \delta \rho_c^0 - iq \cos(\psi) \delta g_{x,0} - iq \sin(\psi) \delta g_{y,0}, \quad (53a)$$

$$\begin{aligned} s \delta g_{x,0} = & \left[\frac{1}{2} iq \cos(\psi) \left(g_0^2 \frac{\mu}{v_2^2} \partial_{\rho_c} v_2 - 1 \right) - g_0 \left(\partial_{\rho_c} v_1 - \frac{\mu\kappa}{v_2^2} g_0^2 \partial_{\rho_c} v_2 \right) \right] \delta \rho_c^0 \\ & + \left(iq \cos(\psi) \frac{\zeta_+}{v_2} g_0 - \frac{q^2}{4v_2} - \frac{2\mu\kappa}{v_2} g_0^2 \right) \delta g_{x,0} + iq \frac{\zeta_-}{v_2} \sin(\psi) g_0 \delta g_{y,0}, \end{aligned} \quad (53b)$$

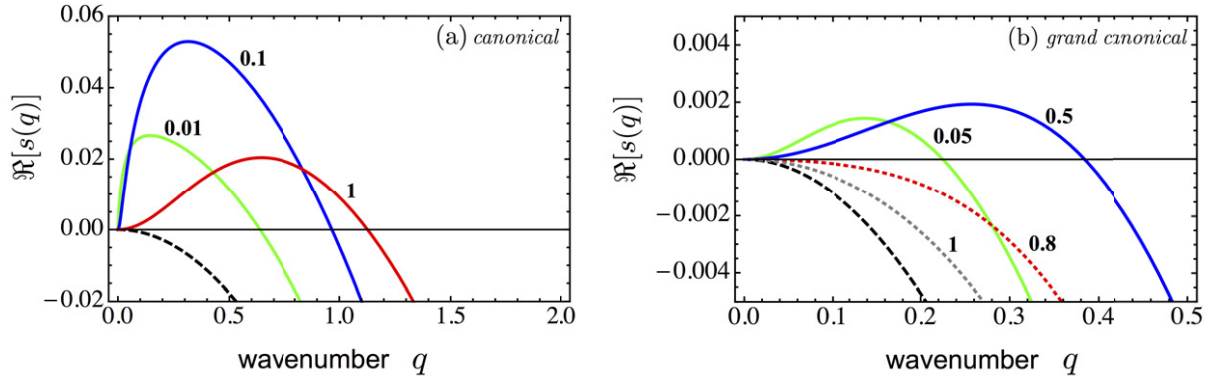


Figure 6. Largest growth rate of $\Re[s(q)]$ as a function of the wavenumber q for $\sigma = 0$ and several values for the total particle density ρ . The marginal $\rho = \rho^{(c)}$ is dashed. Further values are $\rho = \rho^{(c)} + \Delta$ with Δ indicated in the figure. (a) *Canonical model*: for $\rho > \rho^{(c)}$, longitudinal perturbations ($\psi = 0$) are unstable. (b) *Grand canonical model*: transversal ($|\psi| = \pi/2$) perturbations are unstable closely above the critical density $\rho^{(c)}$ (refer to the green and blue curve corresponding to $\Delta \in \{0.05, 0.5\}$). For larger densities, i.e. $\Delta > 0.7$ for $\sigma = 0$, the transversal instability re-stabilizes again (dotted curves, $\Delta \in \{0.8, 1\}$). However, the density regime hosting this transversal instability vanishes completely for noise values larger than σ_r , as illustrated in figure 7.

$$s \delta g_{y,0} = -\frac{1}{2} i q \sin(\psi) \left(g_0^2 \frac{\mu}{v_2^2} \partial_{\rho_c} v_2 + 1 \right) \delta \rho_c^0 - i q \sin(\psi) \frac{\zeta_-}{v_2} g_0 \delta g_{x,0} + \left(i q \cos(\psi) \frac{\zeta_+}{v_2} g_0 - \frac{q^2}{4 v_2} \right) \delta g_{y,0}. \quad (53c)$$

In equations (52a)–(53c) we used $-\nu_1 - \frac{\mu\kappa}{v_2} g_0^2 = 0$, which directly follows from the definition of g_0 , given in equation (39). We numerically solved both eigenvalue problems in the immediate vicinity of the ordering transition line $\rho = \rho^{(c)}(\sigma)$.

In the case of the *canonical* model, we find that the most unstable mode occurs for longitudinal perturbations, i.e. perturbations with wave vectors parallel to the direction of macroscopic motion, $\mathbf{q} \parallel \mathbf{g}_0$ ($\psi = 0$). Figure 6(a) shows the corresponding eigenvalues as functions of the wavenumber q for a set of density values slightly beyond $\rho = \rho^{(c)}$. Further inspection of the coupling coefficients in equations (52a)–(52d) reveals that this longitudinal instability only affects the amplitude of \mathbf{g} leaving the direction unchanged. For $\psi = 0$, the dynamics of $\delta g_{y,0}$ decouples and momentum current density fluctuations perpendicular to the direction of macroscopic motion decay exponentially,

$$\delta g_{y,0} = s_4^{(c)} \delta g_{y,0}, \quad (54)$$

with a rate

$$\Re[s_4^{(c)}] = -\frac{q^2}{4 v_2} < 0, \quad (55)$$

which approaches zero for $q \rightarrow 0$, as expected for a broken symmetry variable. To assess the nature of the instability in greater detail, we calculated the eigenvector corresponding to the

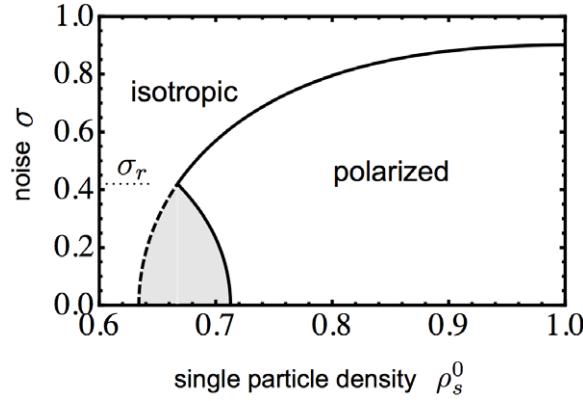


Figure 7. Phase diagram determined from the homogeneous equations of the *grand canonical* model, as a function of noise level σ and single particle density ρ_s^0 , now complemented by the results obtained from the stability analysis of the linearized inhomogeneous equations: whereas longitudinal perturbations decay within the homogeneous phase boundary, there is a zone (gray shaded) where transversal modes become linearly unstable. The width of this zone gradually decreases for increasing noise values σ , and vanishes completely above some critical noise value σ_r (horizontally dotted line).

most unstable longitudinal mode (evaluated at the most unstable wavenumber). It turns out that this eigenvector has approximately equally large components along the remaining fluctuation amplitudes $\delta g_{x,0}$, $\delta \rho_0$ and $\delta \eta_0$. This is consistent with our previous findings, indicating that the density mode, which was alluded to in section 5.2 and which turns unstable at $\rho = \rho_c$, renders the state of homogeneous collective motion unstable to fluctuations of the magnitude of the momentum current density. We further note that this picture is in agreement with previous numerical [31] and analytical [22] results (cf figure 1).

The stability regions of the *grand canonical* model strongly deviate from the above picture. Setting $\psi = 0$ (longitudinal perturbations), we calculated the largest eigenvalue $s_{\max}^{(\text{GC})}$ of the linear system of equations (53a)–(53c):

$$\Re [s_{\max}^{(\text{GC})}] = - \frac{(1 - \rho_s) q^2}{4 \left[(1 - \rho_s)^2 + \rho_s^2 \left(\frac{14}{15} + \frac{2}{3} e^{-2\sigma^2} \right) \right]}, \quad (56)$$

which is always negative since $\rho_s < 1$. In contrast to the *canonical* model, longitudinal perturbations thus always decay exponentially fast in the *grand canonical* model. For perturbations in transverse directions, in contrast, a positive eigenvalue can be found for sufficiently low noise levels $\sigma < \sigma_r$, with the fastest growing modes possessing wave vectors $\mathbf{q} \perp \mathbf{g}_0$. Figure 6(b) shows the eigenvalue of the most unstable modes, which occur for $\sigma = 0$. To assess the implications of this instability for the dynamics of the various fluctuation amplitudes, we numerically examined the eigenvector corresponding to the positive eigenvalue, evaluated at the most unstable wavenumber. For densities in the vicinity of the ordering transition, we find that this eigenvector has approximately equal components in both momentum current density fluctuation amplitudes, $\delta g_{x,0}$ and $\delta g_{y,0}$, but an essentially vanishing component along the direction of density fluctuations $\delta \rho_c^0$. The corresponding instability can thus be classified as a hybrid shear/splay instability, leaving the spatially homogeneously distributed particle density virtually unaffected.

Three remarks are in order. Firstly, for noise values $\sigma_c(\rho \rightarrow \infty) > \sigma > \sigma_r$, the state of homogeneous collective motion becomes linearly stable with respect to arbitrary perturbations, including transverse perturbations. Secondly, even the most unstable eigenvalues ‘restabilize’ for densities that are in the vicinity of the ordering transition threshold, which is depicted in figure 7. Finally, a restabilization can also be ‘observed’ for the longitudinal instability in the *canonical* model. In this case, however, the restabilization occurs for relatively large densities and thus lies outside the range of validity of the linearized equations (52a)–(52d).

6. Discussion and conclusion

To conclude, we discuss and summarize our main findings. To study the onset of collective motion in active media, we started out with a simplified model for a system of self-propelled rod-like particles of variable aspect ratio. Collective motion was assumed to be established in a completely self-organized fashion solely by means of interactions among the constituent particles and in the absence of any external alignment fields. These interactions were assumed to occur via binary, inelastic particle collisions, during which the rods align their direction of motion. Moreover, interactions were assumed to be subject to noise, which we controlled by a single model parameter σ . To assess some of the structural properties of such systems, we associated each of the particles with one of two classes: *single particles* and *cluster particles*, each with the corresponding density fields denoted as ρ_s and ρ_c . The class of *cluster particles* hosts all particles belonging to some coherently moving group of particles, which we referred to as cluster. The rest of the particles can be imagined to make up an isotropic sea of particles and are associated with the class of *single particles*. Using this classification scheme, we implemented simple interaction rules, representing cluster nucleation, cluster growth and cluster evaporation; the latter is assumed to occur at some fixed rate ϵ .

To illuminate the self-organization of collective motion, we set up an analytical, kinetic description of such systems, focusing on two archetypical modeling frameworks. Firstly, we considered isolated systems in which the total number of constituent particles is a conserved quantity. This case was referred to as the *canonical* model. Secondly, we examined open systems, which we referred to as the *grand canonical* model. Open systems are in contact with a particle reservoir which keeps the density of *single particles* at a constant level.

Inspecting the corresponding hydrodynamic equations, we were able to establish the following physical picture, portraying the formation of collective motion via dissipative particle interactions. For both the *canonical* and the *grand canonical* model, we identified two characteristic density scales $\bar{\rho}$ and $\rho^{(c)}(\sigma)$, with $\rho^{(c)}(\sigma) > \bar{\rho}$, which allowed us to distinguish three density regimes.

For low densities, $\rho < \bar{\rho}$, the rate at which particles collide is much smaller than the rate at which clusters disassemble. In terms of a particle-based picture, this regime corresponds to a situation where particle clusters are unstable, evaporating shortly after their nucleation. In the stationary state, the vast majority of particles populates the *single particle* phase, rendering the system homogeneous and isotropic even on mesoscopic scales. This low-density regime terminates at the characteristic density $\bar{\rho}$, where both classes exchange particles at equal rates.

In the contiguous regime of intermediate densities, $\bar{\rho} < \rho < \rho^{(c)}$, the overall rate of cluster formation and growth outstrips the rate at which clusters evaporate, and the majority of particles becomes organized in clusters. Translated to a particle-based notion, clusters grow to finite sizes and persist over macroscopic time scales. Clusters of coherently moving particles now

dominate the physical picture on mesoscopic scales. Yet, interactions among clusters are too rare to establish a macroscopic state of collective motion. On hydrodynamic length scales, the system can be viewed as a homogeneous and isotropic sea of clusters.

For densities exceeding the critical density, $\rho > \rho^{(c)}(\sigma)$, collisions within the cluster phase occur at sufficiently high rates, and macroscopic collective motion emerges. The homogeneous and isotropic state, which has been shown to be stable within the two preceding regimes, thus gets unstable and rotational symmetry is spontaneously broken. Resorting to a particle-based image, we can imagine the mean cluster size to reach a ‘percolation threshold’, leading to coagulation and net alignment between clusters.

While the qualitative features of the *canonical* and the *grand canonical* model are the same in the low and the intermediate density regimes, the establishment of collective motion in the high-density regime differs in important respects in both models. We found that in the *grand canonical* model, a broadly extended region in parameter space exists, where a spatially homogeneous state of macroscopic collective motion exists and is actually stable. Except density, the key parameter controlling the stability of a spatially homogeneous flowing state is the noise amplitude σ . For low noise levels the homogeneous flowing state gets unstable toward transverse perturbations (i.e. perturbations with wave vectors \mathbf{q} perpendicular to the direction of the macroscopic flow). We note, however, that these instabilities are remarkably weak, i.e. the corresponding growth rates are smaller than those of the longitudinal instability in the *canonical* model by a factor of ~ 10 (cf figure 7), and ‘restabilization’ of the spatially homogeneous flowing state occurs upon increasing the density only slightly beyond the threshold $\rho^{(c)}(\sigma)$. Interestingly, this transverse instability vanishes altogether, if angular diffusion is slightly enhanced upon increasing σ . Hence, for intermediate values of σ , the system directly establishes a homogeneous state of collective motion, which is stable against arbitrary perturbations of small magnitude. Finally, if the noise is too strong, order is destroyed and the system remains isotropic even for arbitrarily large densities. This last statement is, of course, shared among all active systems [29], particle conserving or not, and thus applies equally well to the *canonical* model.

In the case of the *canonical* model, a spatially homogeneous base state is unstable toward longitudinal perturbations (i.e. perturbations with wave vectors \mathbf{q} parallel to the direction of the macroscopic flow) for all values of the noise parameter σ . Both the magnitude of the macroscopic velocity field and the particle density are prone to this kind of instability. This is in agreement with previous analytical [22] and numerical [31] results for particle conserving systems, where the emergence of solitary wave structures has been reported in the vicinity of the ordering transition $\rho \gtrsim \rho^{(c)}(\sigma)$. The longitudinal instability thus seems to be a quite generic feature of particle conserving systems with hard core interactions. For an interesting counter example we refer the reader to [26], where a particle conserving system with topological interactions has been studied.

We can now combine our findings for both the *canonical* and the *grand canonical* model to offer the following mechanistic explanation concerning the emergence of the longitudinal instability. The prerequisite, underlying the establishment of coherent motion, is embodied by two basic processes: cluster nucleation by collisions among *single particles* and cluster growth by alignment of *single particles* to clusters. Only if, by virtue of these processes, the concentration of *cluster particles* grows sufficiently large, clusters are able to synchronize their movements by coagulation and macroscopic collective motion emerges.

Now consider the effect of a density fluctuation in an otherwise homogeneous state of macroscopic collective motion. In the *grand canonical* model, where the density of *single*

particles is kept fixed by virtue of a particle reservoir, this fluctuation occurs within the class of *cluster particles*. We can use the right-hand side of equation (35a) to assess the implications of such a fluctuation on the local composition of the system in terms of *cluster particles* and *single particles*:

$$(\rho_s^0 + \rho_c)\rho_s^0 = \rho_c. \quad (57)$$

Note that this equation captures the balance of the two particle currents between the *single particle* and the *cluster particle* phase in the stationary limit. As can be seen from this equation, locally enhancing the density of *cluster particles* implies a net current from the *cluster particle* phase into the *single particle* phase, thus counteracting the effect of the original density fluctuation. Conversely, locally diminishing the density of *cluster particles* leads to the opposite effect. Density fluctuations are thus damped in the *grand canonical* model and do not impact the macroscopic velocity field, which is set up by the *cluster particles*.

Exactly the opposite happens in the particle conserving *canonical* model. Again, consider a spatially homogeneous base state of macroscopic collective motion. Particles are then distributed among the phases of *cluster particles* and *single particles* as determined by the balance equation (cf (34b))

$$\rho(\rho - \eta) = \rho + \eta, \quad (58)$$

where the left-hand side describes cluster nucleation and condensation, and the right-hand side corresponds to cluster evaporation. This can be seen by using the definitions of the relative density $\eta = \rho_c - \rho_s$ and the total particle density $\rho = \rho_s + \rho_c$. Now, consider a fluctuation in the total density ρ , where, for the sake of simplicity, we assume the relative density η to remain constant. In regions where the fluctuation leads to an increase in the total density by a factor $k > 1$, we have

$$k\rho(k\rho - \eta) > k\rho + \eta. \quad (59)$$

Hence, the particle current into the *cluster particle* phase grows. As a consequence, the local value of the momentum current density increases, since the *cluster particles* are the ‘carriers’ of the macroscopic momentum. In contrast, in regions where the fluctuation decreases the total density by a factor $k' < 1$, we have

$$k'\rho(k'\rho - \eta) < k'\rho + \eta. \quad (60)$$

There the *cluster particle* phase gets depleted and the local magnitude of the momentum current density declines. As a result, high-density regions move at faster speeds than low-density regions, gathering more and more particles on their way through the system. Conversely, lower density regions continually lose particles to the faster high-density structures. In particle conserving systems, every density fluctuation thus automatically triggers a corresponding fluctuation in the momentum current density, which in turn amplifies the density fluctuation. As a result of this process, high-density bands of collectively moving *cluster particles* might emerge [31]. These bands are interspersed by regions where the particle density has fallen below the critical density $\rho^{(c)}$ (and possibly below $\bar{\rho}$), leading to local destruction of clusters and collective motion.

We close by adding some remarks on the importance of the particles’ shape on the establishment of collective motion on hydrodynamic scales. We found that the impact of particle shape on the macroscopic properties of such systems is purely quantitative in the framework of our present study: varying the particles’ aspect ratio results in a shift of the characteristic density

scales $\bar{\rho}$ and $\rho^{(c)}(\sigma)$, which we quantified in equation (37). Qualitatively, our conclusions concerning the macroscopic properties of these systems remain unaffected by a change in the particles' aspect ratio. Note that, in our approach, the aspect ratio basically determines the total scattering cross section and thus 'merely' impacts the rate at which particles collide. We stress, however, that in real systems particle shape is likely to have a profound impact on the entire physical picture of particle interactions, and not just on their rate. The study of those effects lies outside the scope of our present work and would be an interesting topic for future research.

Acknowledgments

The authors thank Simon Weber and Jonas Denk for discussions and a critical reading of our paper. Financial support from the DFG in the framework of the SFB 863 and the German Excellence Initiative via the program Nanosystems Initiative Munich (NIM) is gratefully acknowledged. This research was also supported in part by the National Science Foundation under grant no. NSF PHY11-25915.

Appendix A. Derivation of the Boltzmann collision cylinder for driven rods

In the framework of our Boltzmann-like description, binary collisions, such as equations (3), (6) and (7), occur with a certain rate Γ depending on particle shape (L and d), relative angle of both collision partners $\theta_{12} = |\theta_1 - \theta_2|$ and the constant velocity v . The quantity $\Gamma(L, d, \theta_{12})$ characterizes the collision area per unit time—more commonly referred to as a Boltzmann collision cylinder. On the scale of the Boltzmann equation, binary collisions occur locally, say in an infinitesimal volume element centered at \mathbf{r} . Assume that particle 1 has an orientation θ_1 . Then, $\Gamma(L, d, \theta_{12}) dt$ gives the area around particle 1 in which every particle with orientation θ_2 will collide during a time interval $[t, t + dt]$ with particle 1. As a consequence, $\Gamma(L, d, \theta_{12}) f(\mathbf{r}, \theta_1, t) f(\mathbf{r}, \theta_2, t) d\theta_1 d\theta_2$ equals the number of collisions per unit time and unit area at time t , with $f(\mathbf{r}, \theta, t)$ denoting the one-particle distribution function.

To determine $\Gamma(L, d, \theta_{12})$, we take a microscopic point of view. Since the model employed in this work assigns to each particle a velocity vector pointing along its rod axis, we can distinguish 'head' and 'tail'. Referring to figure A.1, without loss of generality we assume $\pi - \theta_{12} \equiv \theta \in [0, \pi]$ (negative relative angles lead to the same result), and consider the blue rod, with the position of its head indicated by the blue dot. All rods of relative orientation $\theta_{12} = \theta_1 - \theta_2$, and with their heads lying in the area $S = A \cup S_1 \cup S_2$ at time t , will collide with the blue rod during the time interval $[t, t + dt]$. Since A , S_1 and S_2 are disjoint,

$$|S| = |B| + |S_1| + |S_2|, \quad (\text{A.1})$$

where $|X|$ denotes the area of the region X . The respective areas are given by

$$|A| = dt v_{\text{rel}} (L - d) |\sin \theta| = dt v_{\text{rel}} (L - d) |\sin \theta_{12}| \quad (\text{A.2})$$

and

$$|S_2| + |S_1| = dt v_{\text{rel}} d \int_{-\theta}^{\pi-\theta} d\phi \sin(\phi + \theta) = 2 dt v_{\text{rel}} d. \quad (\text{A.3})$$

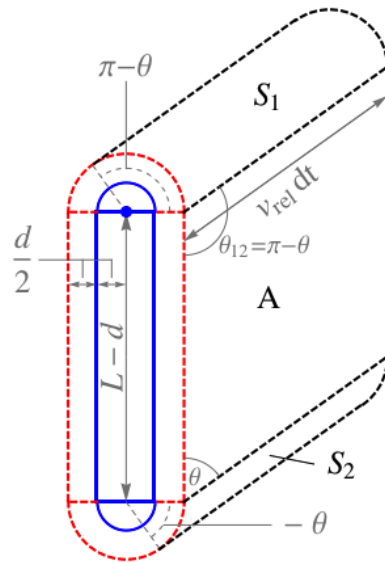


Figure A.1. Illustration of the collision cylinder in the rest frame of the blue rod. The red lines indicate the excluded volume due to the finite expansion of the rods. The quantity v_{rel} denotes the magnitude of the relative velocity of those rods making a relative angle $\theta_{12} = \pi - \theta$ with the blue rod's axis, and is given by $v_{\text{rel}} = v|\hat{\mathbf{e}}(\theta) - \hat{\mathbf{e}}(0)| = 2v|\sin(\theta_{12}/2)|$.

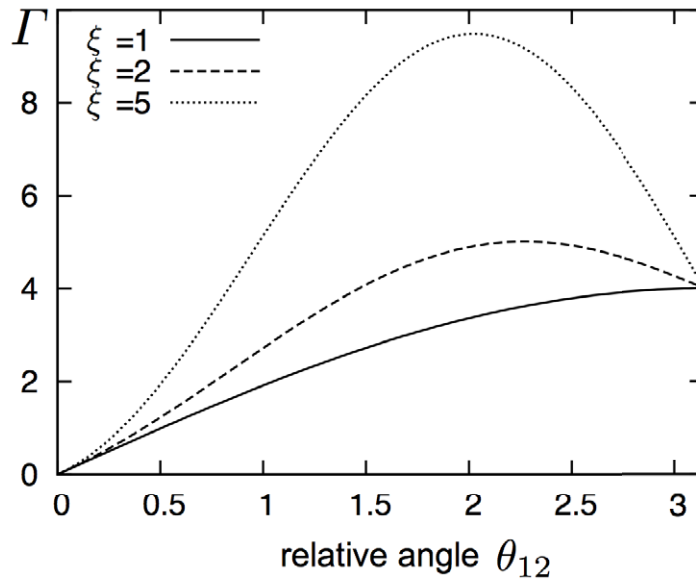


Figure A.2. $\Gamma(L, d, \theta_{12})$ as a function of the relative angle θ_{12} for different values of aspect ratio ξ . For the figure, we chose for particle width $d = 1$ and for particle velocity $v = 1$. Increasing the aspect ratio L/d , the most probable collision approaches $\theta_{12} = \pi/2$, whereas for $L/d = 1$ the most probable collision is the head-head collision with $\theta_{12} = \pi$.

Returning to the laboratory frame we have $v_{\text{rel}} = v|\hat{\mathbf{e}}(\theta_1) - \hat{\mathbf{e}}(\theta_2)| = 2v|\sin(\theta_{12}/2)|$. Noting that $\Gamma = |S|/dt$ (cf equation (A.1)), we find that

$$\Gamma(L, d, \theta_{12}) = 4v d \left| \sin\left(\frac{\theta_{12}}{2}\right) \right| \left(1 + \frac{L/d - 1}{2} |\sin \theta_{12}| \right). \quad (\text{A.4})$$

In figure A.2, $\Gamma(L, d, \theta_{12})$ is shown as a function of relative angle θ_{12} for different particle lengths, whereby the particle width d is kept fixed. Increasing L/d shifts the most probable collision from $\theta_{12} = \pi$ for $L/d = 1$ (the case of a sphere; $\theta_{12} = \pi$ leads to the largest value of the relative velocity) toward $\theta_{12} = \pi/2$ for $L/d \rightarrow \infty$ (limiting case of a needle; largest target area for $\theta_{12} = \pi/2$).

Appendix B. Derivation of the gradient terms in the hydrodynamic equations

To assist the reader in tracing back the emergence of the gradient terms in the hydrodynamic equations (28a)–(28c) (and, likewise, in equations (32a)–(32c) and (33a)–(33c)), we briefly summarize the main steps in the derivation of these equations. All gradient terms in the hydrodynamic equations ultimately arise from the convection term in the first line of equation (24c) and the closure relation obtained by quasi-statically approximating (24d). Here we collect all such (complex) gradient terms and give a brief derivation of their vector-analytic counterparts. As in the main text, we identify \mathbb{C} and \mathbb{R}^2 , i.e.

$$f = f_x + i f_y \in \mathbb{C} \leftrightarrow \mathbf{f} = \begin{pmatrix} f_x \\ f_y \end{pmatrix} \in \mathbb{R}^2. \quad (\text{B.1})$$

To distinguish (genuinely) complex from purely real quantities, we assume $f \in \mathbb{C}$ and $\rho \in \mathbb{R}$ in the following.

$(\partial_x + i\partial_y)\rho$:

Using (B.1) we immediately obtain

$$(\partial_x + i\partial_y)\rho \equiv \nabla \rho. \quad (\text{B.2})$$

$(\partial_x - i\partial_y)(\partial_x + i\partial_y)f$:

By straightforward expansion we find

$$(\partial_x - i\partial_y)(\partial_x + i\partial_y)f = (\partial_x^2 + \partial_y^2)f \equiv \nabla^2 \mathbf{f}. \quad (\text{B.3})$$

$(\partial_x - i\partial_y)f^2$:

Decomposing f into real and imaginary parts and expanding, we find

$$\begin{aligned} (\partial_x - i\partial_y)(f_x^2 - f_y^2 + 2if_x f_y) &= \partial_x f_x^2 - \partial_x f_y^2 + 2\partial_y(f_x f_y) + i[\partial_y f_y^2 - \partial_y f_x^2 + 2\partial_x(f_x f_y)] \\ &\equiv 2 \left[\partial_i(f_i f_j) - \frac{1}{2} \delta_{ij} \partial_i \mathbf{f}^2 \right] \mathbf{e}_j \\ &= 2\mathbf{f}(\nabla \cdot \mathbf{f}) + 2(\mathbf{f} \cdot \nabla)\mathbf{f} - \nabla \mathbf{f}^2, \end{aligned} \quad (\text{B.4})$$

where \mathbf{e}_j denotes the j th Cartesian unit vector.

$[(\partial_x + i\partial_y)f][(\partial_x - i\partial_y)\rho]$:

Expanding and collecting real and imaginary parts, we find

$$[(\partial_x + i\partial_y)f][(\partial_x - i\partial_y)\rho] = \partial_x f_x \partial_x \rho - \partial_y f_y \partial_x \rho + \partial_x f_y \partial_y \rho + \partial_y f_x \partial_y \rho \\ + i(-\partial_x f_x \partial_y \rho + \partial_y f_y \partial_y \rho + \partial_x f_y \partial_x \rho + \partial_y f_x \partial_x \rho).$$

Thus,

$$[(\partial_x + i\partial_y)f][(\partial_x - i\partial_y)\rho] \equiv ((\partial_i f_j) \partial_i \rho + (\partial_j f_i) \partial_i \rho) \mathbf{e}_j - (\nabla \cdot \mathbf{f}) \nabla \rho \\ = [(\nabla \mathbf{f}) + (\nabla \mathbf{f})^T] \nabla \rho - (\nabla \cdot \mathbf{f}) \nabla \rho. \quad (\text{B.5})$$

$$f^2(\partial_x - i\partial_y)\rho:$$

We find

$$f^2(\partial_x - i\partial_y)\rho = f_x^2 \partial_x \rho - f_y^2 \partial_x \rho + 2f_x f_y \partial_y \rho + i(-f_x^2 \partial_y \rho + f_y^2 \partial_y \rho + 2f_x f_y \partial_x \rho).$$

Hence,

$$f^2(\partial_x - i\partial_y)\rho \equiv 2f_i f_j \partial_j \rho \mathbf{e}_i - \mathbf{f}^2 \nabla \rho = 2\mathbf{f}(\mathbf{f} \cdot \nabla \rho) - \mathbf{f}^2 \nabla \rho. \quad (\text{B.6})$$

References

- [1] Ramaswamy S 2010 The mechanics and statistics of active matter *Annu. Rev. Condens. Matter Phys.* **1** 323–45
- [2] Aranson I S and Tsimring L S 2009 *Granular Patterns* (New York: Oxford University Press)
- [3] Marchetti M C, Joanny J-F, Ramaswamy S, Liverpool T B, Prost J, Rao M and Aditi R Simha 2012 Soft active matter arXiv:1207.2929 [cond-mat.soft]
- [4] Butt T, Mufti T, Humayun A, Rosenthal P B, Khan S, Khan S and Molloy J E 2010 Myosin motors drive long range alignment of actin filaments *J. Biol. Chem.* **285** 4964–74
- [5] Schaller V, Weber C A, Semmerich C, Frey E and Bausch A 2010 Polar patterns in propelled filaments *Nature* **467** 73–7
- [6] Schaller V, Weber C, Frey E and Bausch A R 2011 Polar pattern formation: hydrodynamic coupling of driven filaments *Soft Matter* **7** 3213–8
- [7] Zhang H P, Be'er A, Florin E-L and Swinney H L 2010 Collective motion and density fluctuations in bacterial colonies *Proc. Natl Acad. Sci. USA* **107** 13626–30
- [8] Dombrowski C, Cisneros L, Chatkaew S, Goldstein R E and Kessler J O 2004 Self-concentration and large-scale coherence in bacterial dynamics *Phys. Rev. Lett.* **93** 098103
- [9] Schaller V, Weber C A, Hammerich B, Frey E and Bausch A R 2011 Frozen steady states in active systems *Proc. Natl Acad. Sci. USA* **108** 19183–8
- [10] Sumino Y, Nagai K H, Shitaka Y, Tanaka D, Yoshikawa K, Chaté H and Oiwa K 2012 Large-scale vortex lattice emerging from collectively moving microtubules *Nature* **483** 448–452
- [11] Deseigne J, Dauchot O and Chaté H 2010 Collective motion of vibrated polar disks *Phys. Rev. Lett.* **105** 098001
- [12] Deseigne J, Léonard S, Dauchot O and Chaté H 2012 Vibrated polar disks: spontaneous motion, binary collisions, and collective dynamics *Soft Matter* **8** 5629–39
- [13] Kudrolli A, Lumay G, Volfson D and Tsimring L S 2008 Swarming and swirling in self-propelled polar granular rods *Phys. Rev. Lett.* **100** 058001
- [14] Ballerini M *et al* 2008 Empirical investigation of starling flocks: a benchmark study in collective animal behaviour *Animal Behav.* **76** 201–15
- [15] Toner J and Tu Y 1995 Long-range order in a two-dimensional dynamical XY model: how birds fly together *Phys. Rev. Lett.* **75** 4326–9
- [16] Aranson I S and Tsimring L S 2005 Pattern formation of microtubules and motors: inelastic interaction of polar rods *Phys. Rev. E* **71** 050901

- [17] Bertin E, Droz M and Grégoire G 2006 Boltzmann and hydrodynamic description for self-propelled particles *Phys. Rev. E* **74** 022101
- [18] Aranson I S, Sokolov A, Kessler J O and Goldstein R E 2007 Model for dynamical coherence in thin films of self-propelled microorganisms *Phys. Rev. E* **75** 040901
- [19] Baskaran A and Cristina Marchetti M 2008 Hydrodynamics of self-propelled hard rods *Phys. Rev. E* **77** 011920
- [20] Baskaran A and Cristina Marchetti M 2008 Enhanced diffusion and ordering of self-propelled rods *Phys. Rev. Lett.* **101** 268101
- [21] Holm D D, Putkaradze V and Tronci C 2008 Kinetic models of oriented self-assembly *J. Phys. A: Math. Theor.* **41** 344010
- [22] Bertin E, Droz M and Grégoire G 2009 Hydrodynamic equations for self-propelled particles: microscopic derivation and stability analysis *J. Phys. A: Math. Theor.* **42** 445001
- [23] Holm D D, Putkaradze V and Tronci C 2010 Double-bracket dissipation in kinetic theory for particles with anisotropic interactions *Proc. R. Soc. Lond. A* **466** 2991–3012
- [24] Mishra S, Baskaran A and Cristina Marchetti M 2010 Fluctuations and pattern formation in self-propelled particles *Phys. Rev. E* **81** 061916
- [25] Ihle T 2011 Kinetic theory of flocking: derivation of hydrodynamic equations *Phys. Rev. E* **83** 030901
- [26] Peshkov A, Ngo S, Bertin E, Chaté H and Ginelli F 2012 Continuous theory of active matter systems with metric-free interactions *Phys. Rev. Lett.* **109** 098101
- [27] Peshkov A, Aranson I S, Bertin E, Chaté H and Ginelli F 2012 Nonlinear field equations for aligning self-propelled rods *Phys. Rev. Lett.* **109** 268701
- [28] Wensink H H, Dunkel J, Heidenreich S, Drescher K, Goldstein R E, Löwen H and Yeomans J M 2012 Mesoscale turbulence in living fluids *Proc. Natl Acad. Sci. USA* **109** 14308–13
- [29] Vicsek T, Czirók A, Ben-Jacob E, Cohen I and Shochet O 1995 Novel type of phase transition in a system of self-driven particles *Phys. Rev. Lett.* **75** 1226–9
- [30] Czirók A and Vicsek T 2000 Collective behavior of interacting self-propelled particles *Physica A* **281** 17–29
- [31] Grégoire G and Chaté H 2004 Onset of collective and cohesive motion *Phys. Rev. Lett.* **92** 025702
- [32] Chaté H, Ginelli F, Grégoire G and Raynaud F 2008 Collective motion of self-propelled particles interacting without cohesion *Phys. Rev. E* **77** 046113
- [33] Chaté H, Ginelli F, Grégoire G, Peruani F and Raynaud F 2008 Modeling collective motion: variations on the Vicsek model *Eur. Phys. J. B* **64** 451–6
- [34] Grossman D, Aranson I S and Ben Jacob E 2008 Emergence of agent swarm migration and vortex formation through inelastic collisions *New J. Phys.* **10** 023036
- [35] Baglietto G and Albano E V 2009 Nature of the order–disorder transition in the Vicsek model for the collective motion of self-propelled particles *Phys. Rev. E* **80** 050103
- [36] Ginelli F, Peruani F, Bär M and Chaté H 2010 Large-scale collective properties of self-propelled rods *Phys. Rev. Lett.* **104** 184502
- [37] Peruani F, Deutsch A and Bär M 2006 Nonequilibrium clustering of self-propelled rods *Phys. Rev. E* **74** 030904
- [38] Peruani F, Klauss T, Deutsch A and Voss-Boehme A 2011 Traffic jams, gliders and bands in the quest for collective motion of self-propelled particles *Phys. Rev. Lett.* **106** 128101
- [39] Weber C A, Schaller V, Bausch A R and Frey E 2012 Nucleation-induced transition to collective motion in active systems *Phys. Rev. E* **86** 030901
- [40] Lovely P S and Dahlquist F W 1975 Statistical measures of bacterial motility and chemotaxis *J. Theor. Biol.* **50** 477–96
- [41] Toner J, Tu Y and Ramaswamy S 2005 Hydrodynamics and phases of flocks *Ann. Phys.* **318** 170–244